Title

STRUCTURE AND MECHANICAL PROPERTIES OF Fe-Cr-Mo-C ALLOYS WITH AND WITHOUT BORON

Author

Thomas, G.

Publication Date

1979-05-01

Lawrence Berkeley Laboratory
UNIVERSITY OF CALIFORNIA, BERKELEY, CA

Materials & Molecular Research Division

Submitted to Metallurgical Transactions

STRUCTURE AND MECHANICAL PROPERTIES OF Fe-Cr-Mo-C ALLOYS WITH AND WITHOUT BORON

G. Thomas and Yen-Lung Chen

May 1979

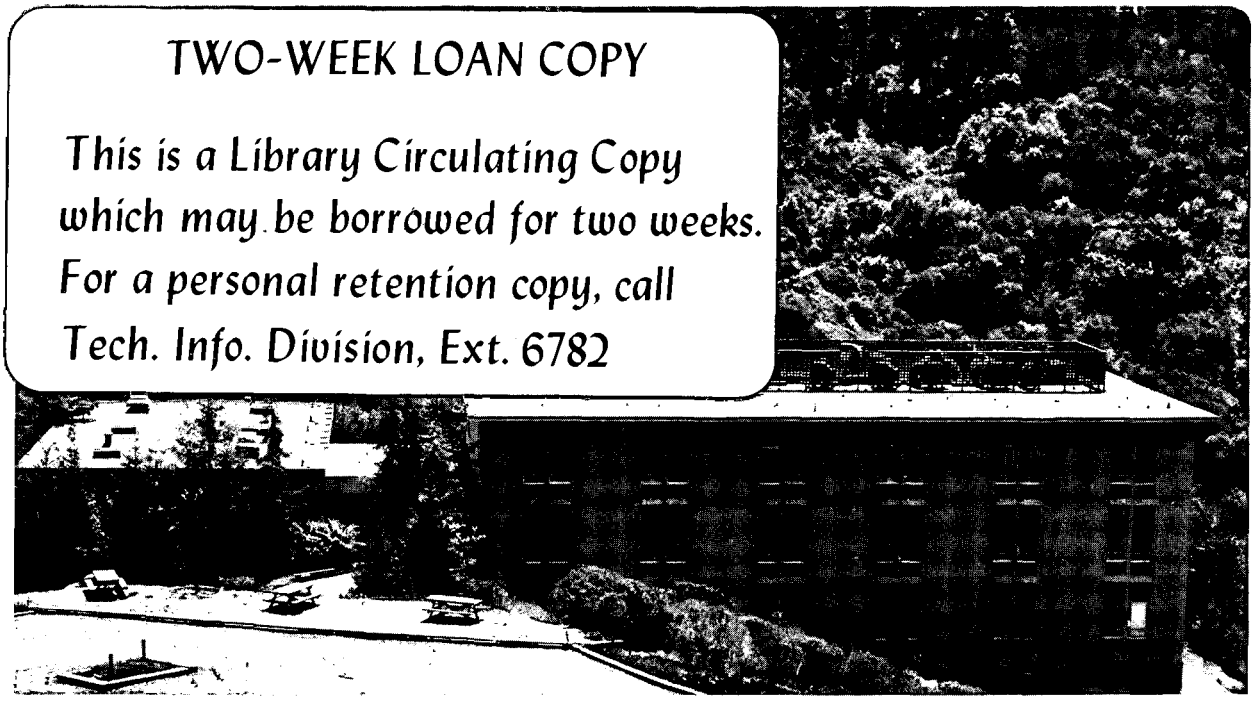

Prepared for the U. S. Department of Energy
under Contract W-7405-ENG-48

DISCLAIMER

STRUCTURE AND MECHANICAL PROPERTIES OF Fe-Cr-Mo-C ALLOYS WITH AND WITHOUT BORON

G. Thomas and Yen-Lung Chen*

Materials and Molecular Research Division, Lawrence Berkeley Laboratory
and Department of Materials Science and Mineral Engineering,
University of California, Berkeley, California 94720

ABSTRACT

A study of the structure and mechanical properties of Fe-Cr-Mo-C martensitic steels with and without boron addition has been carried out. Non-conventional heat treatments have subsequently been designed to improve the mechanical properties of these steels.

Boron has been known to be a very potent element in increasing the hardenability of steel, but its effect on the structure and mechanical properties of quenched and tempered martensitic steels has not been clear. The present results show that the as-quenched structures of both steels consist mainly of dislocated martensite. In the boron-free steel, there are more lath boundary retained austenite films. The boron-treated steel shows higher strengths at all tempering temperatures but with lower Charpy V-notch impact energies. Both steels show tempered martensite embrittlement when tempered at 350°C for 1 hour. The properties above 500°C tempering are significantly different in the two steels. While the boron-free steel shows a continuous increase in toughness when tempered above 500°C, the boron-treated steel suffers a second drop in toughness at 600°C tempering. Transmission electron microscopy studies show that in the 600°C tempered boron-treated steel large, more or less continuous cementite films are present at the lath boundaries, which are probably responsible for the embrittlement. The differences in

---

*Present Address: National Taiwan Institute of Technology, Dept. of Mechanical Engineering and Technology, Keelung Road, Taipei, Taiwan, R.O.C.

mechanical properties at tempering temperatures above 500°C are rationalized in terms of the effect of boron-vacancy interactions on the recovery and recrystallization behavior of these steels.

Althgugh boron seems to impair room temperature impact toughness at low strength levels, it does not affect this property at high strength levels. By simple non-conventional heat treatments of the present alloys, martensitic steels may be produced with quite good strength-toughness properties which are much superior to those of existing commercial ultra-high strength steels. It is also shown that very good combinations of strength and toughness can be obtained with as-quenched martensitic steels.

I. INTRODUCTION

In the on-going design program concerned with strong, tough martensitic steels in our group at Berkeley the role of substitutional alloying elements and heat treatments on the microstructure and mechanical properties is now quite well established[1,2] and can be controlled. In the present research we are concerned with more dilute alloys than those studied previously (total substitutional alloy content <2½%)and in particular the influence of (small amounts of) boron (>0.0005%) has been examined, because of its effectiveness in hardenability[3] and hence great potential in materials conservation[4] and cost savings.[5] The composition is designed to ensure the formation of dislocated (lath) martensite on quenching.

The effectiveness of boron additions on the hardenability decreases as the carbon content of the steel increases and the maximum benefit from boron additions is achieved with low carbon steels.[5-8] A mechanism of the boron hardenability effect has been proposed to be due to the surface absorption of boron onto the prior austenite grain boundaries.[9-12] It is therefore possible that boron contributes to the hardenability of boron-treated steels by a reduction of the interfacial energy of austenite grain boundaries and therefore would retard ferrite nucleation at these sites. The effectiveness of boron in increasing hardenability depends, in addition to the amount, on the form of boron retained in the steel, this form being influenced by the presence of other elements. Boron has a high affinity for oxygen and nitrogen. For the boron added to be effective it is necessary that either the amount of oxygen and nitrogen in the steel be reduced to extremely low levels by the steel making practice or else that they be neutralized by combination with strong oxide and nitride forming elements such as Al, Ti, and Zr.[13]

The solubility of boron in iron is extremely small,[14] but its magnitude and mechanism are still controversial.[15-17] Some experiments suggest an interstitial solution while others show substitutional behavior. The low atomic number of boron makes it difficult to study its distribution in the microstructure by X-ray micro-analysis. Direct evidence of boron partition in the microstructure of steels was not available until the advent of boron autoradiography. This method has the required sensitivity and resolution to determine the boron distribution.[18,19] Natural boron contains 18.8% ^{10}B and 81.2% ^{11}B. The ^{10}B isotope has a thermal neutron capture cross-section of 4010 barns for the reaction $^{10}B(n,\alpha)^{7}Li$. The liberated energy of 2.31 MeV is divided between the reaction products in inverse ratio to their masses, $E_\alpha/E_{Li} = 1.75$.[18] Cellulose acetobutyrate (CAB) was proved to be sensitive to α particles emitted from thermal neutron reactions with the ^{10}B isotope yet insensitive to β and γ radiation.[18] The autoradiographic method using CAB as the detector was therefore employed for the study of boron distribution in the microstructures of the steels in the present research.

Apart from the strong influence on the hardenability of ferritic steels boron has also been known to be beneficial to the hot-working characteristics, creep strength and ductility of creep-resisting steels.[20-22] Although the effect of boron on the hardenability of plain carbon and low-alloy steels has been well established and utilized in commercial practice, its influence on the structure and mechanical properties of martensitic steels is not clear. It is one of the purposes of this research to study the effect of boron on the microstructure and mechanical properties of quenched and tempered martensitic steels. To accomplish this, steels of the same base composition with and without boron addition are compared. Since high strength low alloy (HSLA) steels are important structural materials, and for adequate hardenability, steels of Fe-1Cr-1Mo-0.3C base composition have been chosen.

II. EXPERIMENTAL PROCEDURE

A. Alloy Preparation and Heat Treatment

The two steels were received as hot-rolled plates. The compositions of the alloys are listed in Table 1. P1085 and P1086 alloys were prepared and provided by the Climax Molybdenum Company. The alloys were vacuum melted in 55 lb. heats and carbon deoxidized, using electrolytic iron and ferroalloys for melting materials. The ingots were forged at 1204°C (2200°F) to 3 inches wide and 1½ inches thick slabs. The slabs were then hot rolled to 3/4 inch plates with a reheating temperature of 1093°C (2000°F). All plates were flattened by pressing at about 1093°C. All pieces were sand-blasted, homogenized under vacuum at 1200°C for 24 hours. Tensile specimen blanks and Charpy bars cut from the 3/4 inch plates were austenitized in an argon atmosphere at 1200°C for one hour and then quenched into vigorously agitated iced water, and transferred immediately into liquid nitrogen for one hour. Tempering was conducted in closely controlled neutral salt baths at 200°, 350°, 500°, 600°, and 700°C respectively for one hour and followed by water quenching to room temperature. The transformation temperatures determined by dilatometry (theta dilatronic 111R) are given in Table II.

In addition, variations in heat treatment were investigated to improve mechanical properties. Four heat treatments were designed and conducted, which are listed in Table V.

B. Mechanical Testing

Flat tensile specimens were tested at room temperature in a 5000 Kg capacity Instron Testing Machine at 0.1 cm/min. cross-head speed. Elongations after fracture were determined from a set of inked gage marks scribed onto each specimen with a vernier height gage before testing. Each tensile datum point is the mean of at least two tests. Error bars are shown in the plotted graphs (Figs. 11 and 12).

The standard Charpy V-notch specimens were used. All tests were conducted at room temperature (20°C).

C. Jominy End-quench Testing

Subsized ½ inch dia. Jominy end-quench test bars were used since the standard size (1 inch in diameter) bars could not be obtained. Specimens were machined from bars which were normalized at 900°C for 1 hour. These specimens then were encapsulated in quartz tubes with 10 inch Hg argon back-fill. Specimens were austenitized at 870°C or 1200°C for 40 min. and then quenched in the Jominy end-quench test apparatus. Two mutually parallel surfaces were wet-ground on each bar and Rockwell "C" hardness measurements were conducted in accordance to ASTM specifications.[23]

D. Metallography

Optical, scanning electron (JSM-U3 microscope) and transmission electron microscopy were carried out on all samples. Specimen preparation was done in the usual manner.[24] Thin foils were prepared from Charpy specimens. X-ray (CuK_{α}) and electron microscope analyses of all specimens were also carried out.

E. Boron Autoradiography

Although Auger spectroscopy studies were carried out on fractured specimens (fractured in vacuum) no conclusive results were obtained since all fractures were transgranular (with respect to prior austenite) and boron segregation could not be detected. Therefore boron autoradiography was used to determine the distribution of boron in the microstructure.

Specimens for autoradiography were about 3 x 3 x 0.5 mm in size, cut from fractured Charpy specimens, mounted in bakelite and polished using standard optical metallographic procedures. Films of cellulose acetobutyrate

(CAB) 0.075 mm thick were then applied onto the polished specimens with methyl ethyl ketone (MEK). One or two scratches were made on the polished surfaces to facilitate the interpretation of the autoradiographs. The films on the specimens were dried in a desiccator and then heated for 16 hours at 140°C. Specimens were then encapsulated in polyethylene bags. Additional pieces of CAB films were placed over the films on the specimens to protect them from mechanical damage. Specimens were positioned in the thermal neutron column in the TRIGA reactor and exposed to a thermal neutron flux of 4.0 x $10^9 n/cm^2$ -sec for 4 hours. After irradiation the specimens were soaked in distilled water for at least 30 min. so that the films could be easily removed from the specimens without damage. The films were then chemically etched for 30-40 min. image side down in 10M KOH at 50°C, washed with distilled water and mounted dry on microscope slides, covered with cover slips, held in position with adhesive tape. The α tracks in the films were then examined by using phase contrast microscopy.

F. Electron Microprobe Analysis

A small amount of Ti was present in the boron treated steel (to protect boron from reacting with oxygen and nitrogen). Although the amount of titanium added is very small, it was felt necessary to check the distribution of titanium in the microstructure since it has been reported[25,26] that titanium can have a secondary hardening effect if it is in solution in the as-quenched state (when the amount of Ti as then at least 10 times larger than that in P1086 steel). Electron microprobe analyses were carried out on metallographically polished specimens with and without boron in the as-quenched and 600°C tempered specimens. The specimens were examined using a MAC 400 Electron Probe Microanalyzer. The results showed that high titanium

concentrations were present in many undissolved particles. Also from wet-chemical analysis it was found that titanium in solution was less than 0.006%. It is therefore concluded that the amount of titanium in solution is extremely small and its influence on the mechanical properties upon tempering would be negligible.

III. RESULTS

A. Metallography

1. As-Quenched Steels

Optical micrographs from as-quenched fractured Charpy impact specimens are shown in Figs. 1a,b. It is evident that these steels have large prior austenite grain size after the 1200°C austenitizing treatment. The average grain size of P1085 steel is about 530 μm and that of P1086 steel is about 270 μm. Although it has been reported[27,28] that boron has a tendency to promote grain coarsening, the grain refining effect of Ti (which was added for the protection of boron) was strong enough to override this behavior. The spread of grain sizes is large since at high austenitizing temperatures austenite grain coarsening occurs and results in a mixture of coarse and fine grains.[29]

The as-quenched structure appears to be completely martensitic. X-ray diffraction analyses of the as-quenched specimens failed to detect retained austenite. However, as is now known this indicates only that the volume fraction of austenite, if present, is less than ~2%.[30,31]

Transmission electron microscopy studies of the as-quenched structures of P1085 and P1086 steels showed the structure to be mainly dislocated martensite with some auto-tempered carbides. Since the M_s temperatures are high in these steels auto-tempering occurred in spite of the severity of the quench used. These steels were designed not to have too low a M_s

temperature since M_s temperature is known to have an important effect on the type of martensite (dislocated and twinned martensite) formed. Figures 2 and 3 show the dislocated martensite, auto-tempered carbide and highly deformed austenite at the martensite lath boundaries in the as-quenched P1085 and P1086 steels. The lath widths of these alloys varied from 0.1 μ to 2 μ. The structures of P1085 and P1086 steels are quite similar except for the small differences in the amount of lath boundary retained austenite and a minor increase in extent of transformation twinning in P1086. Although in X-ray diffraction work no detectable retained austenite was observed in the as-quenched specimens the transmission electron microscopy study clearly proved the existence of retained austenite films surrounding some of the martensite laths. The details concerning electron diffraction analyses of retained austenite and interlath carbide have been discussed recently[30] and need not be repeated here.

2. Tempered Steels

The structures of the specimens tempered at 200°C were similar to those of the as-quenched specimens except that the carbide density was higher. The Widmanstatten arrays of carbides are parallel to $\{110\}\alpha$ indicating that these carbides are Fe_3C.[32-36] The interlath austenite films were still present after this treatment (Fig. 4).

The microstructures of the 1085 and 1086 steels tempered at 350°C were quite different from the microstructures of the as-quenched and 200°C tempered specimens of both steels. Extensive cementite precipitation both inside the laths and at the lath boundaries was observed (Fig. 5). Figure 5 illustrates that the Fe_3C precipitation at the lath boundaries is the main difference between the 350°C tempered structure, as-quenched, and 200°C tempered structures. Seal and Honeycombe[37] suggest that the absence of Fe_3C precipitation at lath

boundaries in the low tempering temperature range (<400°C) is due to the presence of interlath retained austenite films. They propose that carbides do not form at the martensite interfaces at low tempering temperatures because of the higher solubility of carbon in austenite. Upon tempering at higher temperatures the retained austenite will have transformed and the carbides begin to form at the lath boundaries because of the higher carbon concentration there. The present observation confirms this point, the interlath retained austenite films disappeared and instead carbides on the lath boundaries were observed. Lath boundary precipitation of Fe_3C was observed at even lower tempering temperatures in steels of similar carbon level[38,39] as discussed in more detail elsewhere.[30]

Increasing tempering temperature produced coarsening and some spherodisation and at 600°C considerable recovery of the dislocated martensite structure had occurred.

After 600°C tempering temperature the microstructure of P1085 steel was significantly different from that of P1086 steel (compare Figs. 6,7). As shown in Fig. 6 the cementite precipitates within the lath were quite large (coarsened). Also recovery of the dislocation structure is evident. In Figs. 6c and 6d it was found that M_7C_3 carbide precipitates were also present. Since Fig. 6b was taken using superimposed (021) Fe_3C and (24.0)M_7C_3 reflections (spot A in Fig. 6) it is difficult to distinguish M_7C_3 precipitates from the coarsened cementite particles in Figs. 6a and 6b, but it is possible they are the small particles in Fig. 6, since these cannot be Fe_3C. The diffraction information (d-spacings) prove that M_7C_3 is present.

The orientation relationship between M_7C_3 and ferrite was determined

from the diffraction patterns to be:

$$(00.1)M_7C_3 \;//\; (0\bar{1}\bar{1})_\alpha$$

$$(12.0)M_7C_3 \;//\; (2\bar{1}\bar{1})_\alpha$$

$$[2\bar{1}.0]M_7C_3 \;//\; [111]_\alpha$$

The cementite ferrite relationship is the well established Bagaryatski one.[40]

In P1086 steel tempered at 600°C no M_7C_3 carbides were observed. In contrast to the segmented, partially spheroidized lath boundary carbide particles in P1085 steel, large, more or less continuous cementite precipitates at the lath boundaries were observed in P1086 steel, Fig. 7. From Fig. 7(d) it is clear that the Bagaryatski orientation relationship is obeyed. Recovery of the dislocation structure of P1086 steels is not as evident as in the P1085 steel.

In the P1086 steel tempered at 700°C the so-called "boron constituent"[6,7] forms at the grain boundaries, and is characteristic of boron-treated steels. While recovery and recrystallization processes were prominent in the P1085 steel tempered at 700°C recovery was observed, but not recrystallization, in the 700°C tempered P1086 steel. Large $M_{23}(C,B)_6$ precipitates were found in the latter case, but these were not observed in P1085 steel. The orientation relationship between these $M_{23}(C,B)_6$ precipitates and the ferrite matrix was found to satisfy the Kurdjumov-Sachs relation for BCC and FCC crystal lattices.

B. Fractography

Three modes of fracture were observed in these steels: (a) quasi-cleavage, (b) tearing, and (c) microvoid coalescence fractures.[41-43] The fractographic study indicated that in all the specimens fracture occurred by the operation of various combinations of the above mechanisms. The relative importance of

these depends on the steel and heat treatment. Figure 8 shows dimpled and quasi-cleavage ruptures which are typical of the as-quenched P1085 and P1086 steels. Figure 9 illustrates that in the 350°C tempered P1085 and P1086 steels fracture occurred primarily by the quasi-cleavage mechanism. Tear ridges and river patterns are evident. It is to be noted that a significant change in fracture mode from mainly dimpled rupture to mostly quasi-cleavage fracture occurred as the tempering temperature increased to 350°C. These observations correlate well with the electron microscope results and the mechanical property data shown in Figs. 10-12 especially the impact toughness results of Fig. 12. The tempering embrittlement at 350°C is associated with the interlath decomposition of austenite to form carbides. For specimens tempered at 500°C some dimpled ruptures could again be observed though quasi-cleavage fracture was the dominant fracture mode. It should be noted that the small amount of boron in P1086 steel did not have any influence on thermal stability of retained austenite.

C. Boron Autoradiography

Figures 13, 14 show the boron autoradiographs of P1085 and P1086 steels in different heat-treated conditions. Boron segregation at the prior austenite grain boundaries was found in the as-received, homogenized state, although no precipitate particles at the prior austenite grain boundaries were observed. This segregation probably occurred during the slow cooling following homogenization. Figure 13 shows the difference in boron distribution in the microstructure of P1086 steel austenitized at different temperatures. In the P1086 steel quenched from 1200°C (average grain size 270 μm), boron is uniformly distributed (Fig. 13(b)) and no segregation of boron was observed. While in the as-quenched specimens, austenitized at 870°C (average grain size

$\sim$ 30 μm) boron segregation to the prior austenite grain boundaries can be deduced by comparing the radiographs and metallographic data. Possible such segregation is shown in Fig. 13(d). Such a difference in boron distribution affects the hardenability of P1086 steel, as shown in Figs. 15, 16. Figure 14(a) shows that in the 600°C tempered P1086 steel (austenitized at 1200°C) boron is still uniformly distributed throughout. This would imply that boron influences the tempering behavior of this steel, probably by its interaction with vacancies and/or carbon. Figure 14(b) shows the distribution of boron in the 700°C tempered P1086 steel which was austenitized at 1200°C. A high concentration of boron at the prior austenite grain boundaries again is observed, however, this may be due to the small "boron-constituent" particles at the grain boundaries. In these autoradiographs the large white spots and marks are artifacts of the chemically processed detector films. The finite spread of α-tracks at the grain boundaries is due to the nature of the emission process of α particles. As can be seen the spatial resolution of this method is limited by this spread of α-tracks at the grain boundaries and therefore would not be suitable for the detection of boron segregation at the prior austenite grain boundaries in a fine-grained ($\lesssim$ 10μ) steel.

D. Mechanical Properties

The hardness vs. tempering temperature data for P1085 and P1086 steels are plotted in Fig. 10. While the small differences in Rockwell C hardness values at tempering temperatures up to 600°C can be attributed to the small difference in carbon content of these alloys the significantly large differences at 700°C tempering must be partly due to the differences in recovery and recrystallization behavior.

The room temperature tensile properties are given in Tables III and IV and also shown graphically in Figs. 11(a,b). The values of ultimate strength,

yield strength, elongation, and reduction in area were determined by the conventional methods.

Tempering above 600°C results in a drastic decrease in yield strength, in both the steels, Fig. 11 (a). It is clearly indicated that while there is little difference in strength at lower tempering temperatures (the difference in strength of the as-quenched P1085 and P1086 steels is mainly attributed to the difference in carbon content) there are significant differences at tempering temperatures above 500°C. In the 500-600°C temperature range the strength of P1086 steel showed a "levelling-off", whereas that of P1085 steel continued to decrease at about a constant rate, Fig. 11(a).

The variations of elongation at fracture and uniform elongation with respect to tempering temperature are shown in Fig. 11(b). P1086 steel has a higher total elongation than P1085 steel at lower tempering temperatures (200°-500°C). The values of the uniform elongation of both steels are quite similar at all tempering temperatures. The total elongation and uniform elongation were observed to vary with the tempering temperature in a similar trend. The Charpy fracture properties are shown in Fig. 12 and have been discussed above. The tempered martensite embrittlement at 350°C is associated with the transformation of retained austenite to carbide at the lath boundaries. Upon tempering at higher temperatures P1085 and P1086 steels showed quite a different response. After the minimum at 350°C tempering, the impact energy of P1085 steel increases rapidly on tempering at higher temperatures as can be clearly seen in Fig. 12. The toughness of P1086 steel increases upon tempering at 500°C, followed by another minimum at 600°C tempering, and then another increase on tempering at higher temperatures. The second minimum on the Charpy energy curve of P1086 steel is the main difference between P1085 and P1086 steels in tempering response. This second embrittlement in P1086 steel is not a temper brittleness phenomenon since

the fracture is not intergranular.[44,45]

From Tables III and IV it is observed that high toughness values tend to correspond to high ε_f (true fracture strain) values. This is consistent with the explanation that a tough material has a high capacity for deforming locally in the vicinity of the crack tip, that is, a high ε_f, value. It is clearly shown in Figs. 11(a) and 12 that while there is little difference in Charpy toughness between P1085 and P1086 steels at high strength levels (tempered <500°C), there are significant differences at lower strength levels (tempered >500°C). These are due to the more or less continuous inter-lath carbide films in the 600°C tempered P1086 steel and the absence of recrystallization after the 700°C temper.

E. Hardenability

Figures 15 and 16 show the Jominy end-quench hardenability curves of these steels after austenitizing at 870°C, and at 1200°C, respectively. At lower austenitizing temperatures (870°C) the boron effect on hardenability is quite evident but at higher austenitizing temperature (1200°C) there is little difference in hardenability between the steels. Both steels exhibit lower hardenability after 1200°C, compared to 870°C, treatment. This is unusual behaviour which is not understood.

The little difference in hardenability between these steels austenitized at 1200°C is due to the following: (a) P1085 steel has a larger austenite grain size (ASTM #-2, compared with ASTM-#0 in the P1086 steel), and (b) austenitizing at such a high temperature reduces the degree of boron segregation at prior austenite grain boundaries[3,17] thus decreasing the efficiency of boron as a hardenabilty agent. As seen in Fig. 13, boron is uniformly distributed in the as-quenched structure of the 1200°C austenitized P1086 steel. This effect is sometimes referred to as a "boron fade". However,

the loss in hardenability can be recovered by (a) holding at a lower temperature (in the austenite region) or (b) cooling to room temperature and reaustenitizing at a lower temperature.[5,6,9]

IV. OPTIMIZING HEAT TREATMENTS TO OBTAIN SUPERIOR MECHANICAL PROPERTIES

A great deal of work has been done toward the improvement of ductility and toughness of ultra-high strength steels. The processes may involve an adjustment of chemical composition, uses of conventional and non-conventional heat treatment methods, or thermonmechanical treatments. During the course of this study attempts have also been made to obtain improved mechanical properties, i.e., high strength coupled with good toughness, through the use of some thermal treatments only.[46,47]

Four different heat-treatments were designed and performed as listed in Table V and Fig. 17. The cycle in Fig. 17(b) involves austenitizing at 1200°C for 1 hour, quenching to obtain martnesite, tempering at T_t (200°C was used) and quenching to room temperature. Specimens were then reaustenitized at 870°C for time t (1 hour was used) and quenched again to otain martensite. This method combines the beneficial effects of high austenitizing temperature (more alloying elements in solution) with a fine, uniform grain size, obtained by reaustenitizing at low temperature.[46,47] The underlying principle is that by tempering the initial martensitic structure at low temperatures, fine cementite particles are uniformly distributed throughout the structure. Upon reaustenitizing these fine precipitates act as nucleation centers for austenite and a fine, uniform austenite grain size results. The fine precipitate particles subsequently dissolve in austenite.

The mechanical properties of P1085 and P1086 steels subjected to different heat treatment are given in Table V. The improvement of the strength-impact toughness property due to grain-refining treatments is

also summarized in Fig. 18. It is clear that the best mechanical properties were obtained by using heat treatment No. 2 (Fig. 17(b)). Figure 1 shows the optical micrographs of the steels, comparing the prior austenite grain sizes as a function of different heat treatments. It is observed that heat treatment No. 2 gives uniform, fine grains as expected (Figs. 1(c) and 1(d)). The grain sizes of the steels subjected to other heat treatments are larger and vary over a large range. Also it is to be noted that in Fig. 18 the data of heat treatment No. 2 lie on the top edge of the upper hand. This method can be developed further by varying T_t and t (Fig. 17(b)) and further improvements in mechanical properties are expected.

Transmission electron microscopy shows that in heat treatment Nos. 2-4 the amount of interlath retained austenite increases significantly over that of heat treatment No. 1. The stabilization of austenite by fine prior austenite grain size has been observed by other investigators.[48,2] Figure 19 shows an example of extensive lath boundary retained austenite films in the steels subjected to these heat treatments. In P1086 steel the amount of retained austenite is smaller than that in P1085 steel. Fractography showed that the percentage of shear fracture and the size of shear lip depend upon the steel and heat treatment. In steels subject to heat treatments 2-4 the fracture was almost completely dimpled rupture. Thus the grain-refining heat treatments are very beneficial in improving the impact toughness of these steels. A comparison of the strength impact toughness property of these grain-refined alloys with several commonly used commercial ultra-high strength steels has been made and is shown in Fig. 20. It is clear that fine-grained P1085 and P1086 steels possess much superior strength-impact toughness properties to those of the existing highly alloyed and more complex commercial steels.

V. SUMMARY AND CONCLUSIONS

Based on this study of the structure and mechanical properties of Fe-Cr-Mo-C alloys with and without boron additions the following conclusions are made.

A. Effects of Boron

1. Boron increases the hardenability of Fe-1Cr-1Mo-0.3C alloy at low austenitizing temperature (870°C), but not at 1200°C.

2. Boron has almost no effect on the martensite transformation temperatures, and the microstructures tempered below 500°C, of the Fe-Cr-Mo-C alloys studied.

3. The as-quenched structures of both steels consist mainly of dislocated martensite with inter-lath boundary retained austenite and some auto-tempered carbide particles. In the boron-free steel there appears to be more lath boundary retained austenite.

4. In the specimens austenitized at 1200°C boron is uniformly distributed in the microstructure while in the specimens austenitized at 870°C boron segregation to the prior austenite grain boundaries is evident.

5. Boron-treated steel has a higher tempering resistance than the boron-free steel, especially at tempering temperatures above 500°C.

6. Boron-treated steel shows inferior room temperature Charpy V-notch impact toughness than the boron-free steel, especially following tempering at temperatures above 500°C.

7. Tempered martensite embrittlement at 350°C tempering in both steels is attributed to the preferential cementite precipitation at the martensite lath boundaries, due to decomposition of the austenite.

8. In the boron-treated steel, tempering at 600°C leads to the precipitation of large, more or less continuous cementite films at lath boundaries. This is probably responsible for the embrittlement after 600°C tempering.

9. At 600°C tempering temperature, recovery of dislocation substructures is evident in the boron-free steel while in the boron-treated steel the dislocation density remains high. After tempering at 700°C, the boron-free steel shows extensive recovery and the beginning of recrystallization, while in the boron-treated steel although recovery is observed recrystallization is not found.

B. Optimization of Heat Treatment

1. Considerably improved strength-impact toughness properties can be developed in the low alloy steels investigated in the present study by simple, nonconventional heat treatments. Heat treatment No. 2 is the best to date and can be undoubtedly be further developed. The as-quenched steels are not necessarily brittle and in fact, quite good combinations of strength and impact toughness can be obtained with as-quenched martensitic steels.

2. The improved impact toughness at similar strength levels was due to (a) fine, uniform grain size, (b) extensive lath boundary retained austenite films. The low temperature intermediate tempering gives uniformly distributed fine carbides which act subsequently as nucleation centers for austenite upon reaustenitizing at 870°C, and result in fine, uniform grain sizes. The beneficial effect of interlath retained austenite film is probably due to its ability, being a ductile, tough phase, to blunt the crack tips and retard the crack propagation.

VI. ACKNOWLEDGEMENTS

This work was supported by the Division of Materials Sciences, Office of Basic Energy Sciences, U.S. Department of Energy. One of the authors (Y-L Chen) was granted a Fellowship by the Ministry of Education, Republic of China. We are grateful to Dr. B. V. N. Rao for helpful discussion during the course of this work. Alloys P1085 and P1086 were kindly donated by the Climax Molybdenum Co., through the courtesy of Dr. W. C. Hagel.

Table I. Chemical Composition of the Alloys Used (given in Wt.%)*

Alloy No.	C**	Mn	Si	Cr	Mo	B	Ti	Al
P1085	0.25	0.32	0.10	1.00	1.00	---	---	0.029
P1086	0.28	0.30	0.08	1.00	0.97	0.0016	0.016	0.022

* Alloys and data provided by Climax Molybdenum Company.

**Carbon Analysis was measured after Homogenization.

Table II. Phase Transformation Temperatures

Alloy No.	A_s,°C	A_f,°C	M_s,°C
P1085	792	847	378
P1086	791	844	370

Table III. Mechanical Properties of P1085 Alloy Tested at Room Temperature.

Tempering Temp., °C	Ultimate Tensile Strength ksi(MPa)	0.2% Offset Yield Strength ksi(MPa)	Elongation* %	Reduction in Area%	Strain Hardening Coeff. n	True Fracture Strain ε_f	Charpy V-notch Impact Energy Ft-lb_f(N-M)
As-quenched	234 (1614)	199 (1372)	5.4 (2.7)	29	0.027	0.337	27.7 (37.6)
200	224 (1544)	189 (1303)	6.4 (2.8)	41	0.028	0.531	24.9 (33.8)
350	191 (1317)	172 (1186)	5.9 (2.5)	38	0.025	0.485	13.6 (18.4)
500	175 (1207)	157 (1083)	6.9 (3.0)	42	0.030	0.545	26.9 (36.5)
600	166 (1145)	148 (1021)	11.4 (4.8)	62	0.047	0.962	53.4 (72.4)
700	117 (807)	99 (683)	13.6 (6.5)	66	0.063	1.079	133.5 (181.0)

*Values of percent elongation to fracture and percent uniform elongation (in parantheses) are given.

Table IV. Mechanical Properties of P1086 Alloy Tested at Room Temperature

Tempering Temp., °C	Ultimate Tensile Strength ksi(MPa)	0.2% Offset Yield Strength ksi(MPa)	Elongation* %	Reduction in Area%	Strain Hardening Coeff. n	True Fracture Strain ε_f	Charpy V-notch Impact Energy Ft-lb$_f$(N-W)
As-quenched	268 (1848)	221 (1524)	5.5 (3.0)	30	0.030	0.360	27.2 (36.9)
200	229 (1579)	194 (1338)	7.8 (2.9)	46	0.029	0.624	18.0 (24.4)
350	197 (1358)	175 (1207)	7.1 (2.2)	50	0.022	0.693	6.3 (8.5)
500	184 (1269)	164 (1131)	8.2 (3.3)	52	0.032	0.736	18.5 (25.0)
600	182 (1255)	164 (1131)	9.9 (4.5)	52	0.044	0.738	10.0 (13.6)
700	146 (1007)	131 (903)	10.9 (5.5)	56	0.054	0.814	35.0 (47.5)

*Values of percent elongation to fracture and percent uniform elongation (in parantheses) are given.

Table V. Effect of Heat Treatment on Mechanical Properties

Alloy No.	Heat Treatment*	Ultimate Tensile Strength ksi (MPa)	0.2% Offset Yield Strength ksi (MPa)	Elongation+ %	Reduction in Area %	Strain Hardening Coeff. n	True Fracture Strain ε_f	Charpy V-notch Impact Energy Ft-lb_f(N-M)
P1085	1	234 (1614)	199 (1372)	5.4 (2.7)	29	0.027	0.337	27.7 (37.6)
	2	246 (1696)	196 (1352)	8.9 (3.0)	60	0.030	0.911	42.0 (57.0)
	3	240 (1655)	195 (1345)	8.4 (3.0)	52	0.030	0.734	38.5 (52.2)
	4	256 (1765)	202 (1393)	8.8 (3.6)	46	0.035	0.622	32.2 (43.7)
P1086	1	268 (1848)	221 (1524)	5.5 (3.0)	30	0.030	0.360	27.2 (36.9)
	2	273 (1882)	220 (1517)	8.2 (2.7)	61	0.027	0.931	39.4 (53.4)
	3	268 (1848)	215 (1483)	7.1 (3.0)	54	0.030	0.768	27.1 (36.7)
	4	267 (1841)	217 (1496)	8.9 (3.6)	55	0.035	0.792	29.5 (40.0)

*1-- 1200°C x 1 Hr, iced water quenched.
2-- 1200°C x 1Hr, iced water quenched + 200°C x 1 Hr tempering + 870°C x 1 Hr, iced water quenched.
3-- 870°C x 1Hr, iced water quenched.
4-- 1200°C x 1 Hr, iced water quenched + 870°C x 1 Hr, iced water quenched.

+Values of percent elongation to fracture and percent uniform elongation (in parentheses) are given.

REFERENCES

1. G. Thomas: Iron and Steel International, 1973, vol. 46, p. 451.
2. B. V. Narasimha Rao and G. Thomas: Met. Trans. A (in press).
3. D. T. Llewellyn and W. T. Cook: Metals Tech., 1974, Vol. 1, p. 517.
4. R. A. Grange: Boron in Iron and Steel, Part I of B, Ca Cb and Zr in Iron and Steel, John Wiley and Sons, New York, 1957.
5. S. J. Matas: The Role of Boron in Steel, Republic Steel Research Center, Cleveland (Ohio), Project 12046-16, January 27, 1970.
6. R. A. Grange and J. B. Mitchell: Trans. ASM, 1961, vol. 53, p. 157.
7. R. A. Grange and T. M. Garvey: Trans. ASM, 1946, vol. 37, p. 136.
8. G. D. Rahrer and C. D. Armstrong: Trans. ASM, 1948, vol. 40, p. 1099.
9. C. R. Simcoe, A. R. Elsea, and G. K. Manning: Trans. AIME, 1955, vol. 203, p. 193.
10. J. W. Spretnak and R. Speiser: Trans. AIME, 1953, vol. 197, p. 445.
11. A. M. Adair, J. W. Spretnak, and R. Speiser: Trans. AIME, 1955, vol. 203, p. 353.
12. J. C. Fisher: Trans. AIME, 1954, vol. 200, p. 1146.
13. B. M. Kapadia, R. M. Brown, and W. J. Murphy: Trans. TMS-AIME, 1968, vol. 242, p. 1689.
14. Metals Handbook, 8th ed., vol. 8, American Society for Metals, Metals Park, Ohio, 1973, p. 270.
15. Y. Hayashi and T. Sugeno: Acta Met., 1970, vol. 18, p. 693.
16. A. Lucci and G. Venturello: Scripta Met., 1971, vol. 5, p. 17.
17. A. Brown, J. D. Garnish, and R. W. K. Honeycombe: Metal Sci., 1974, vol. 8, p. 317.
18. J. D. H. Hughes and G. T. Rogers: J. Inst. Metals, 1967, vol. 95, p. 299.

19. J. D. Garnish and J. D. H. Hughes: J. Mat. Sci., 1972, vol. 7, p. 7.

20. P. G. Stone: in High Temperature Properties of Steels, Publication 97, Iron and Steel Inst., London, p. 505, 1967.

21. F. B. Pickering: Iron and Steel, 1968, vol. 41, p. 296..

22. T. W. Williams, D. R. Harries, and J. Furnival: JISI, 1972, Vol. 210, p. 351.

23. Annual Book of ASTM Standards, Designation: A255-67, p. 99, 1974.

24. G. Thomas: Transmission Electron Microscopy of Metals, J. Wiley and Sons, New York, 1962.

25. K. Nishida: Trans. ISIJ, 1969, vol. 9, p. 313.

26. K. Kuo: JISI, 1956, vol. 184, p. 258.

27. R. S. Archer: Metal Prog., 1946, vol. 50, p. 677.

28. A. E. Powers and R. G. Carlson: Trans. ASM, 1954, vol. 46, p. 483.

29. T. Gladman and F. B. Pickering: JISI, 1967, vol. 205, p. 653.

30. G. Thomas: Met. Trans. A, 1978, vol 9A, p. 439.

31. R. L. Miller: Trans. ASM, 1964, vol 57, p. 892.

32. M. Raghavan and G. Thomas: Met. Trans., 1971, vol. 2, p. 3433.

33. S. Das and G. Thomas: Trans. AMS, 1969, vol. 62, p. 659.

34. P. M. Kelly and J. Nutting: Proc. Roy. Soc., 1960, vol. A259, p. 45.

35. P. M. Kelly and J. Nutting: in Physical Properties of Martensite and Bainite, ISI Spec. Rpt. No. 93, The Iron and Steel Institute, London, p. 166, 1965.

36. E. Page, P. Manganon, G. Thomas and V. Zackay: Trans. ASM, 1969, vol. 62, p. 45.

37. A. K. Seal and R. W. K. Honeycombe: JISI, 1958, vol. 188, p. 9.

38. R. D. Goolsby: Ph.D. Thesis, University of California, Berkeley, California, 1971.

39. D. H. Huang and G. Thomas: Met. Trans., 1971, vol. 2, p. 1587.

40. Yu. A. Bagaryatski, Dokl. Akad. Nauk: S.S.S.R., 1950, vol. 73, p. 1161.

41. C. D. Beachem and R. M. N. Pelloux: in Fracture Toughness Testing and Its Applications, ASTM STP 381, American Society for Testing and Materials, Philadelphia, p. 210, 1965.

42. W. A. S. Spitzig, in Electron Microfractography, ASTM STP 453, American Society for Testing and Materials, Philadelphia, p. 90, 1968.

43. Metals Handbook, 8th ed., vol. 9, Fractography and Atlas of Fractographs, American Society for Metals, Metals Park, Ohio, 1974, p. 64.

44. C. J. McMahon, Jr.: in Temper Embrittlement in Steel, ASTM STP 407, p. 127, 1968.

45. J. R. Low, Jr.: Trans. TMS-AIME, 1969, vol. 245, p. 2481.

46. B. V. N. Rao and G. Thomas: Mat. Sci. and Eng., 1975, vol. 20, p. 195.

47. B. V. N. Rao, R. W. Miller and G. Thomas: Proc. 16th Int'l Heat Treatment Conf., The Metals Soc., London, 1976, p. 75.

48. W. C. Leslie and R. L. Miller: Trans. ASM, 1964, vol. 57, p. 972.

FIGURE CAPTIONS

Fig. 1. Showing prior austenite grain sizes of P1085 and P1086 steels after different heat treatments. (a) P1085 steel, after heat treatment No. 1, grain size ~ASTM #-2. (b) P1086 steel, after heat treatment No. 1, grain size ~ASTM #0. (c) P1085 steel, after heat treatment No. 2, grain size ~ASTM #7-9. (d) P1086 steel, after heat treatment No. 2, grain size ~ASTM #7-9.

Fig. 2. Alloy P1085, as quenched. Bright field image (a) shows dislocated martensite with lath boundary retained austenite. Dark field image (b) was taken using $(\bar{2}00)_\gamma$ reflection: the lath boundary retained austenite reverses contrast, (c) shows the selected area diffraction pattern and (d) the indexed pattern.

Fig. 3. Alloy P1086, as quenched. Bright field image (a) shows dislocated martensite and lath boundary retained austenite. (b) Dark field image using an austenite reflection: the lath boundary retained austenite reverses contrast.

Fig. 4. Showing lath boundary retained austenite of the 200°C tempered P1085 steel. Cementite and ε-carbide particles can also be seen in the bright field image (a). Dark field imaging using an austenite reflection shows the reversal of contrast of the lath boundary retained austenite, as shown in (b).

Fig. 5. Alloy 1085, quenched and tempered at 350°C. Bright field image (a) and dark field image (b) show cementite precipitation both within martensite laths and at the lath boundaries.

Fig. 6. Alloy P1085, quenched and tempered at 600°C. (a) Bright field image shows coarsened cementite particles and the

precipitation of M_7C_3 carbide. (b) Dark field image using superimposed $(021)_{Fe3C}$ and $(24.0)_{M7C3}$ reflections, shows the reversal of contrast of these carbides. Since the superimposed beams were used for imaging, as shown in the selected area diffraction pattern (c) analyzed in (d) it was not possible to distinguish cementite from M_7C_3 carbide. The reflection used for dark field imaging is marked A in Fig. (d).

Fig. 7. Alloy P1086, quenched and tempered at 600°C. (a) Bright field image reveals no obvious lath boundary carbide precipitation, while in the dark field image (b) of a cementite reflection large, more or less continuous cementite films at the lath boundaries show up very clearly, (c) shows the selected area diffraction pattern and (d) the indexing.

Fig. 8. Fractograph showing a mixture of dimpled and quasi-cleavage fractures in the as-quenched P1086 steel.

Fig. 9. Fractograph showing quasi-cleavage fracture of the 350°C tempered P1086 steel.

Fig. 10. Rockwell C hardness vs. tempering temperature curves of P1085 and P1086 steels.

Fig. 11a. Showing the strength variation of P1085 and P1086 steels as a function of tempering temperature.

Fig. 11b. Showing the elongation of P1085 and P1086 steels as a function of tempering temperature.

Fig. 12. Charpy impact energy variations with tempering temperature. All tests were done at 20°C.

Fig. 13. Boron autoradiographs of P1085 and P1086 steels after different heat treatments. (a) P1085 steel, as quenched from 1200°C x 1 hr. (b) P1086 steel, as quenched from 1200°C x 1 hr.

No segregation of boron was observed. Prior austenite grain size ~270 μm. (c) P1085 steel, as quenched from 870°C x 1 hr. (d) P1086 steel, as quenched from 870°C x 1 hr. Boron segregation to the prior austenite grain boundaries is evident. Prior austenite grain size ~30 μm.

Fig. 14. Boron autoradiographs. (a) P1086 steel quenched from 1200°C x 1 hr, and tempered at 600°C for 1 hr. No segregation of boron was observed. (b) P1086 steel quenched from 1200°C x 1 hr, and tempered at 700°C for 1 hr. Segregation of boron to the prior austenite grain boundaries was again observed, however, this may be due to the small "boron-constituent" particles at the grain boundaries (c.f. Fig. 10).

Fig. 15. Hardenability curves of P1085 and P1086 steels. Austenitizing temperature of these steels was 870°C.

Fig. 16. Hardenability curves of P1085 and P1086 steels. Austenitizing temperature of these steels was 1200°C.

Fig. 17. (a) Shows the conventional heat treatment and (b) shows the experimental heat treating method.

Fig. 18. Showing the strength-impact toughness characteristics of the experimental steels and the effect of grain refinement on the strength-toughness properties of P1085 and P1086 steels.

Fig. 19. Showing extensive lath boundary retained austenite in P1085 steel subjected to heat treatment No. 2. In bright field image (a) the retained austenite does not have good contrast, however, in the dark field image (b) of an austenite reflection the lath boundary retained austenite shows up very clearly.

Fig. 20. Comparison of Charpy impact energy values of the experimental steels with several commercial ultra-high strength steels (Data of commercial steels are from R. T. Ault, G. M. Wald, and R. B. Bertolo, Tech. Rep. AFML-TR-71-27, 1971).

Fig. 20. Comparison of Charpy impact energy values of the experimental steels with several commercial ultra-high strength steels (Data of commercial steels are from R. T. Ault, G. M. Wald, and R. B. Bertolo, Tech. Rep. AFML-TR-71-27, 1971).

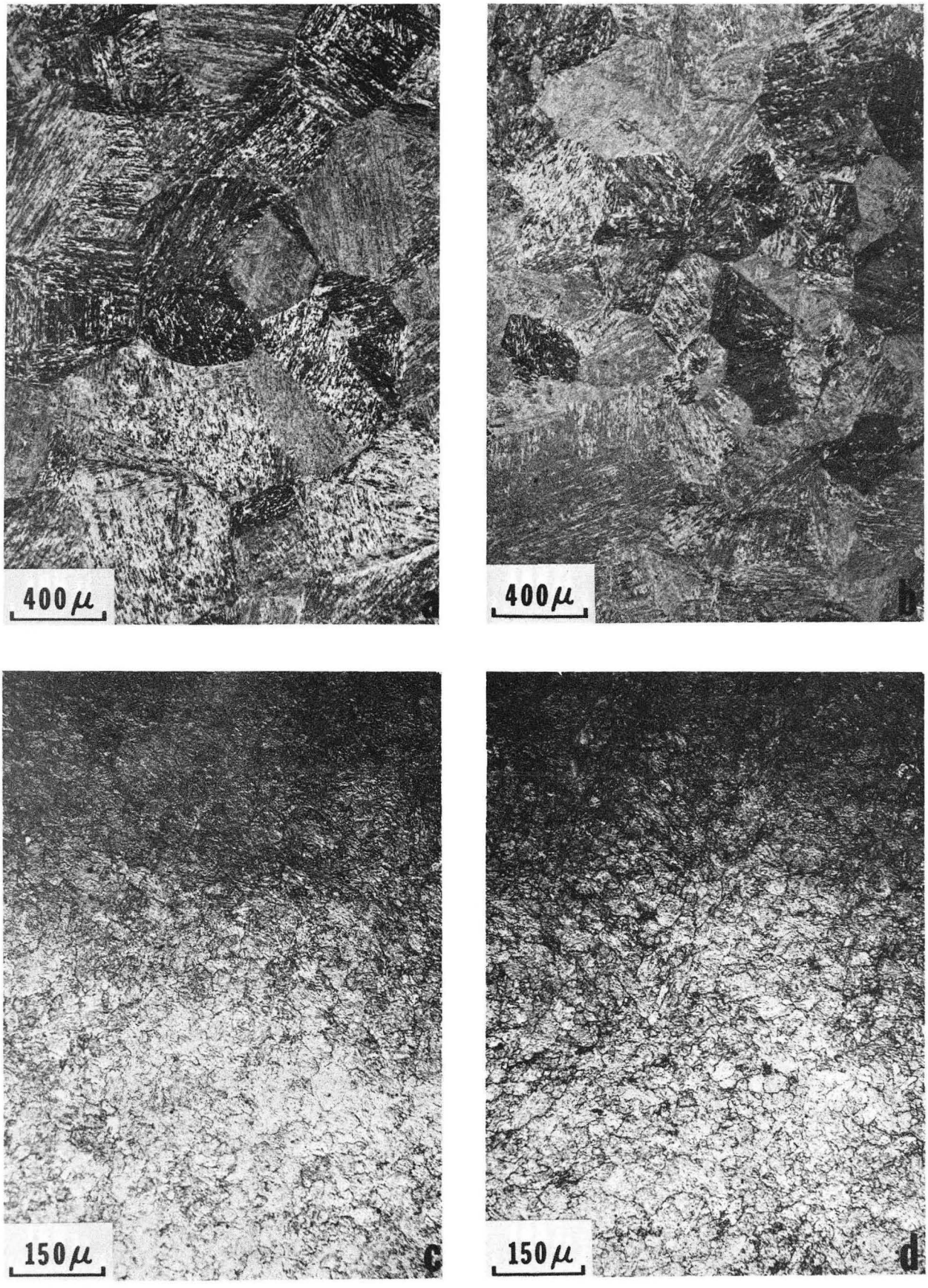

XBB 764 3838

Fig. 1

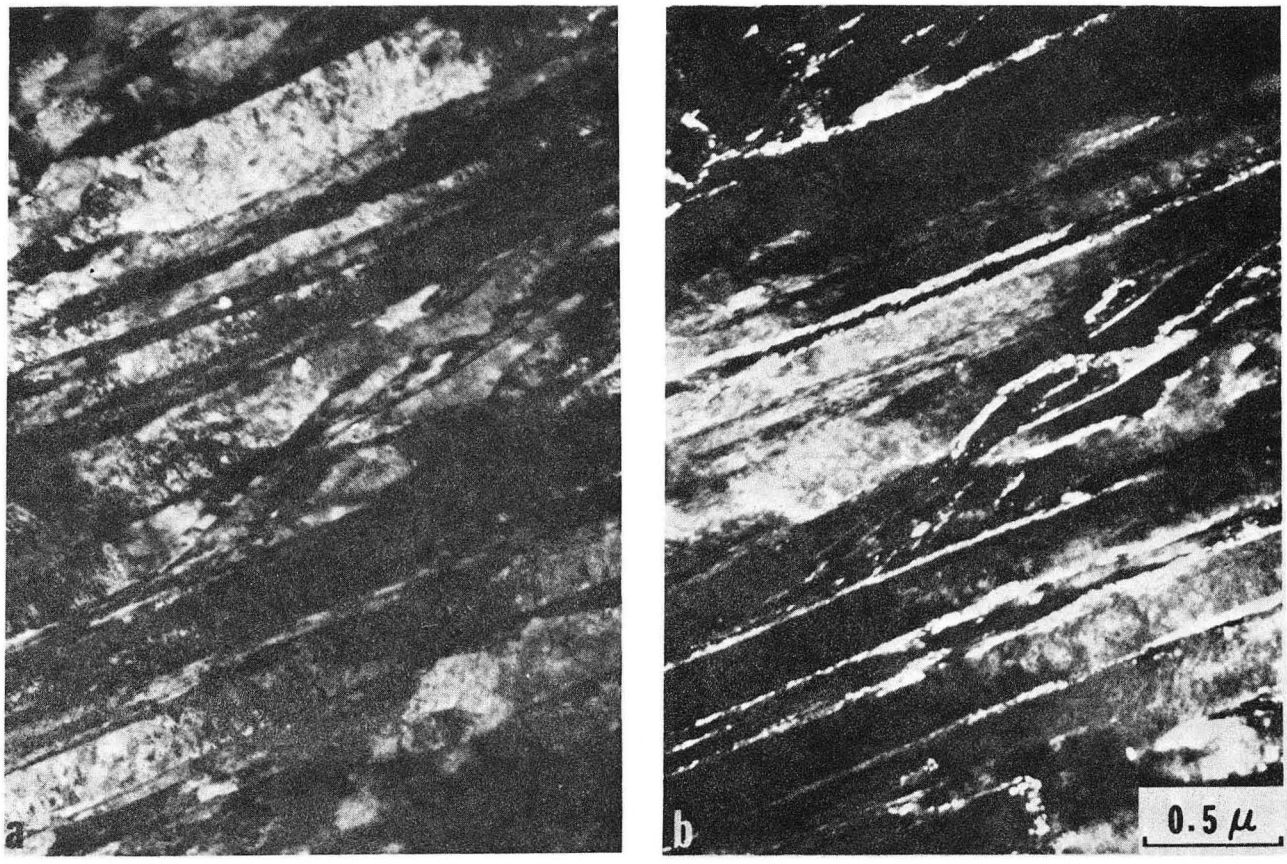

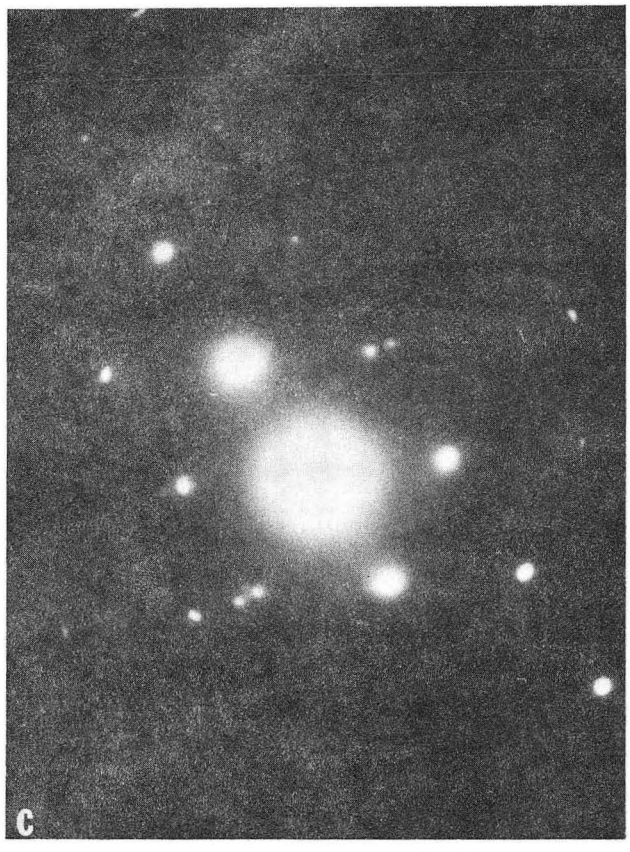

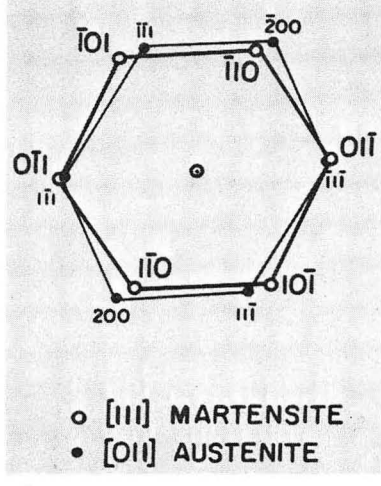

d

Fig. 2

XBB 765 3917

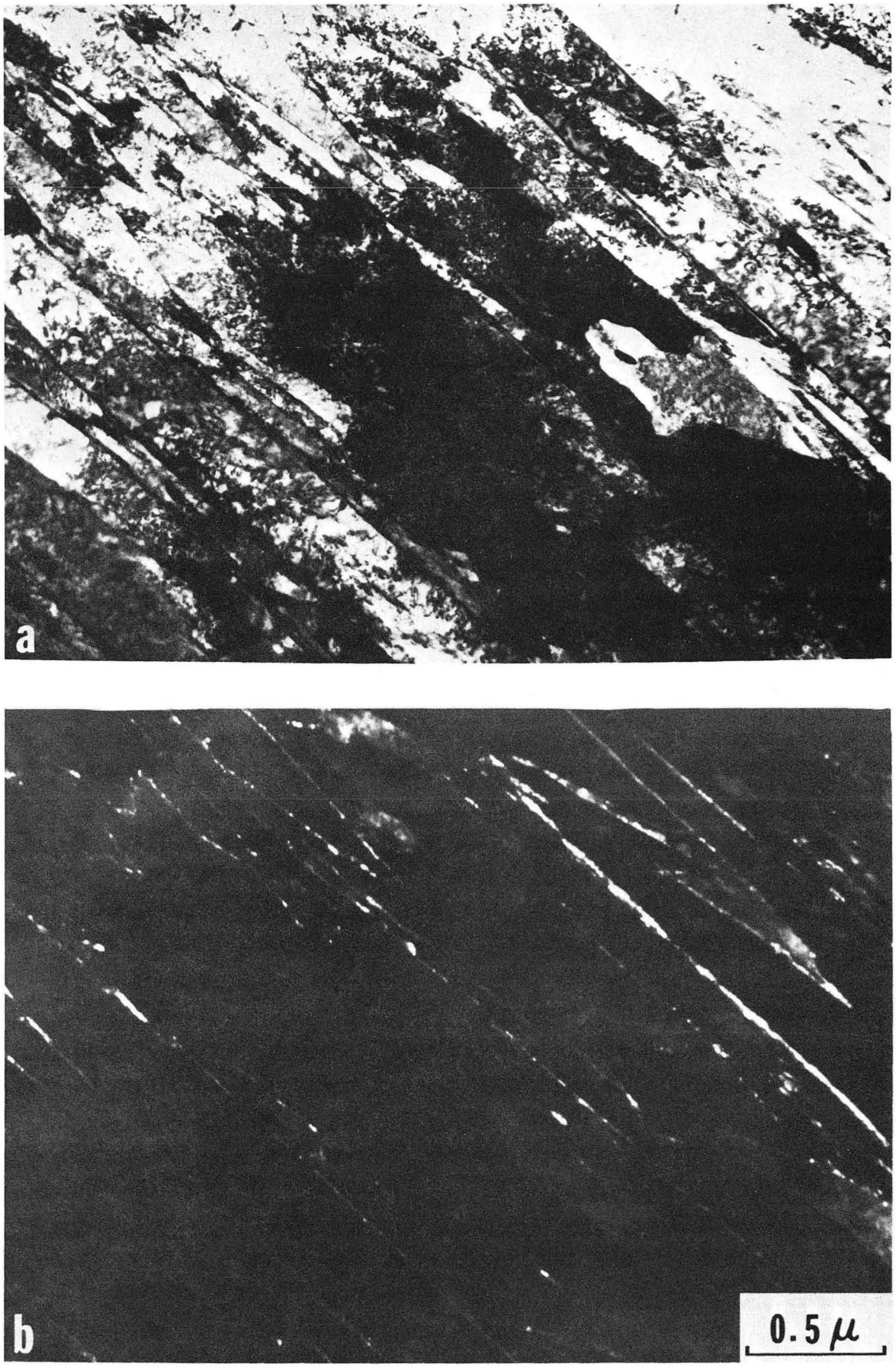

Fig. 3

XBB 765 3912

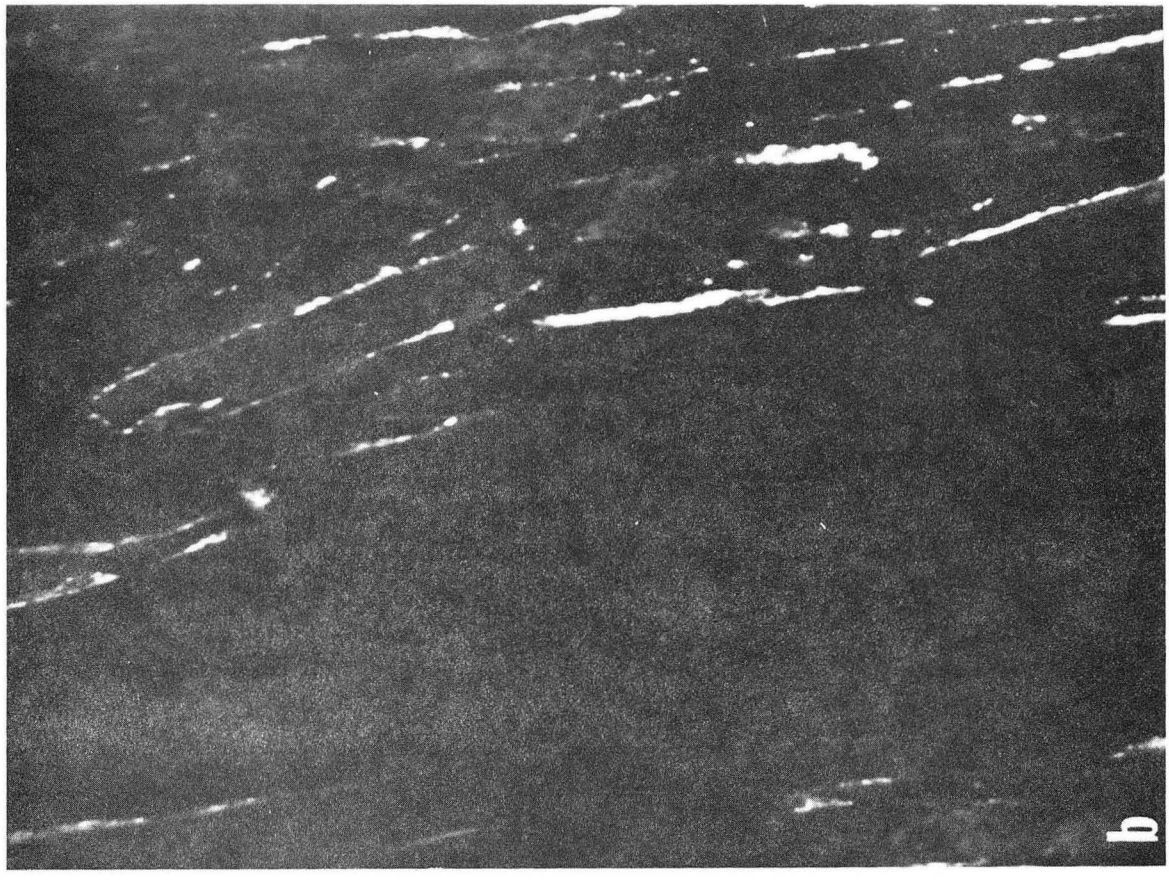

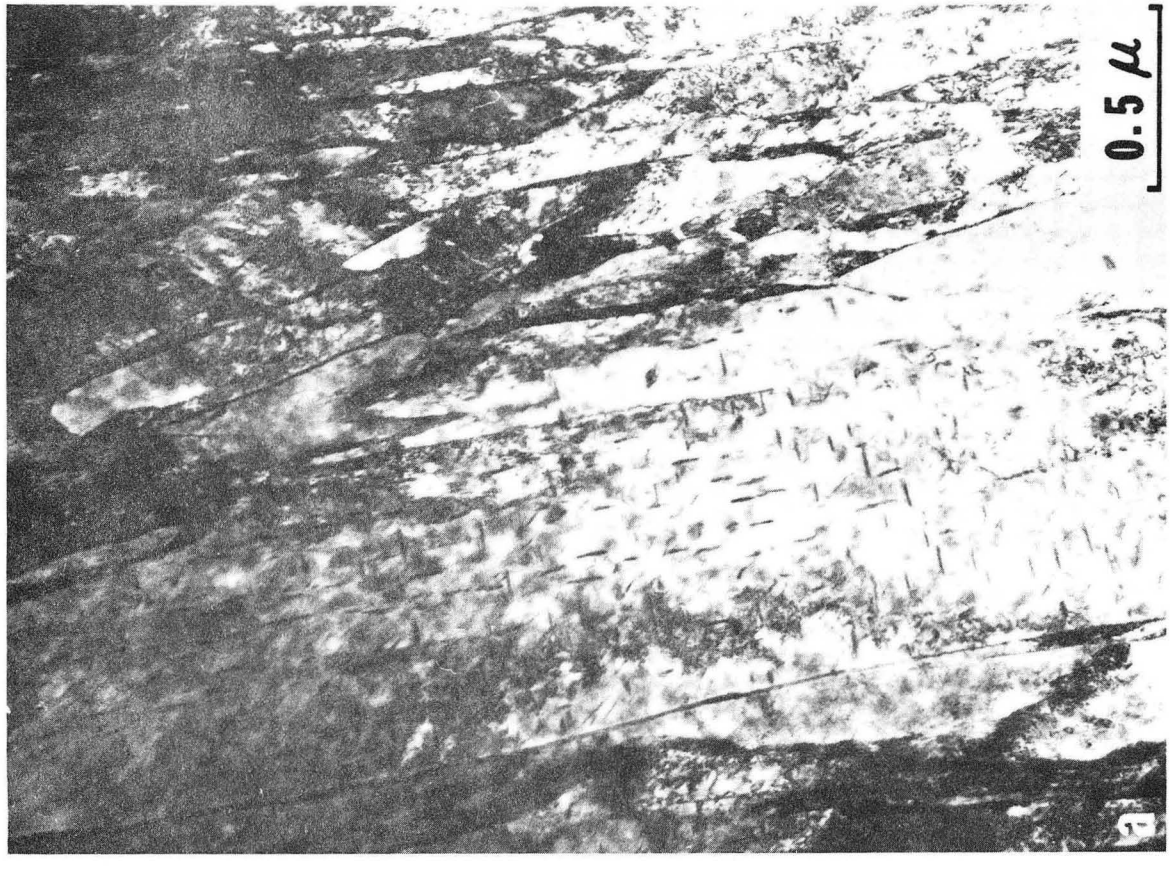

XBB 765 3911

Fig. 4

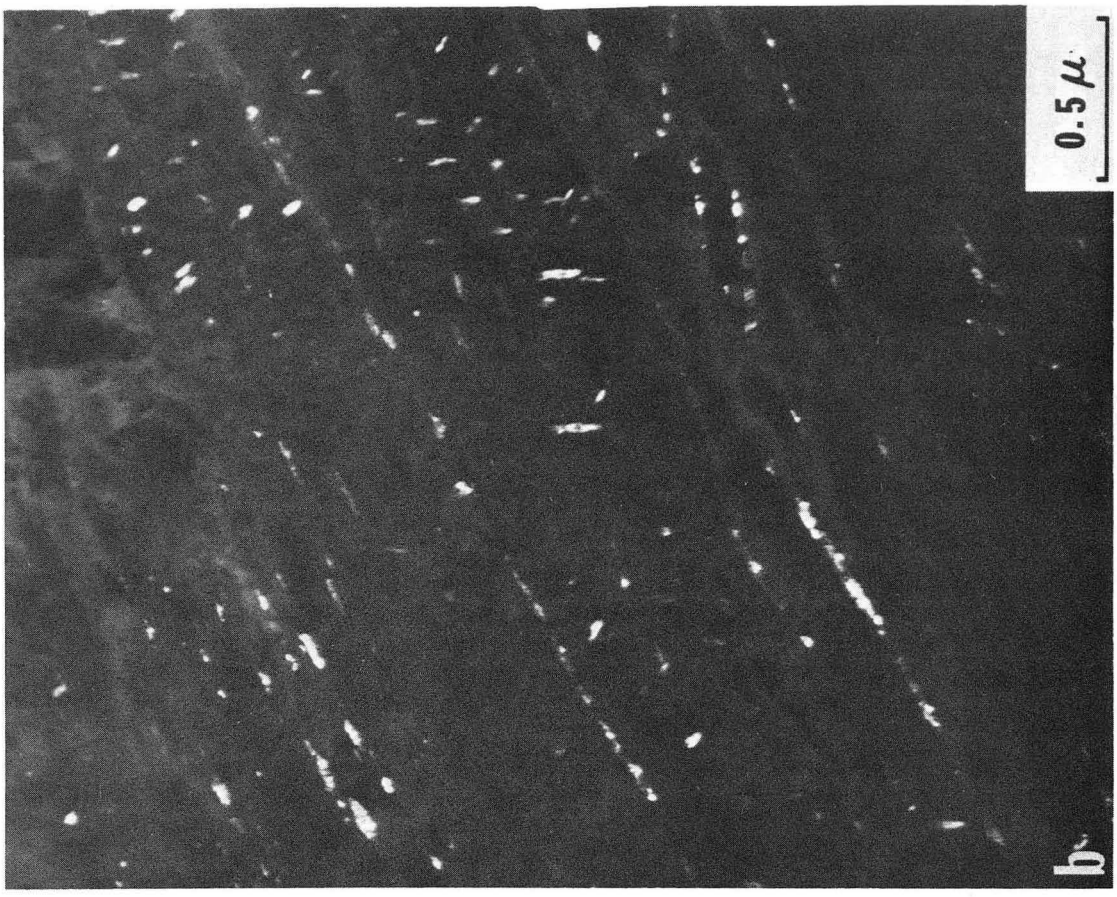

XBB 755 3725

Fig. 5

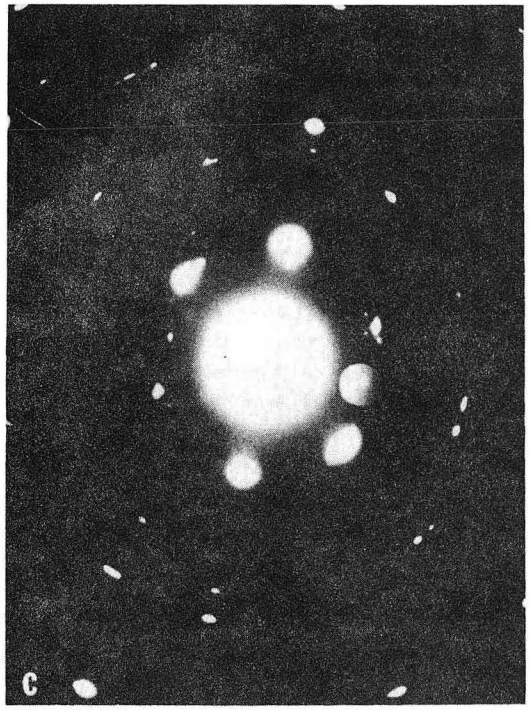

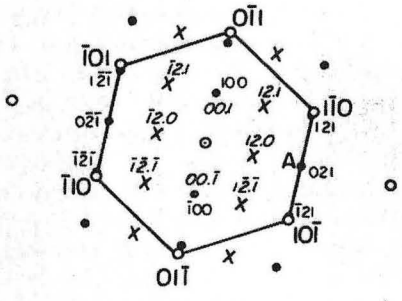

XBB 765-3915

Fig. 6

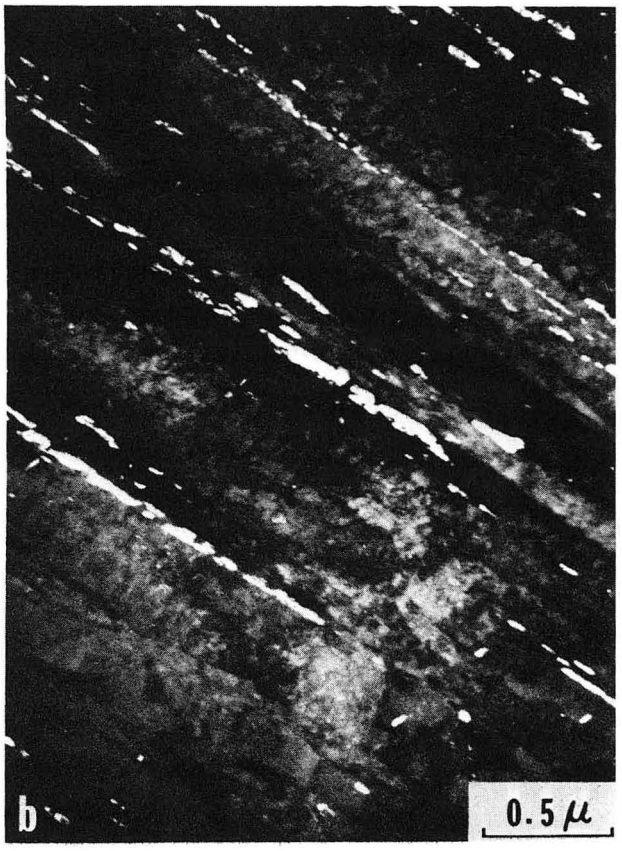

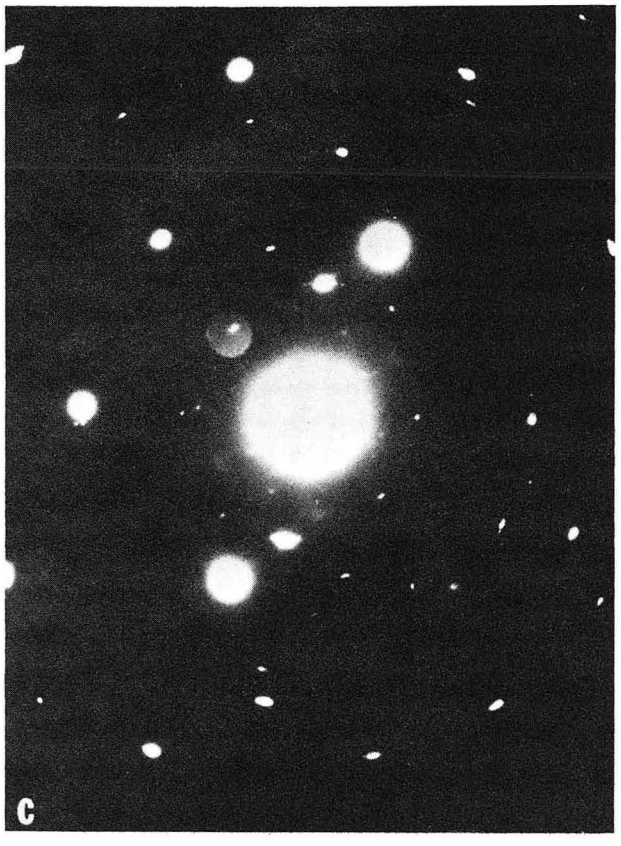

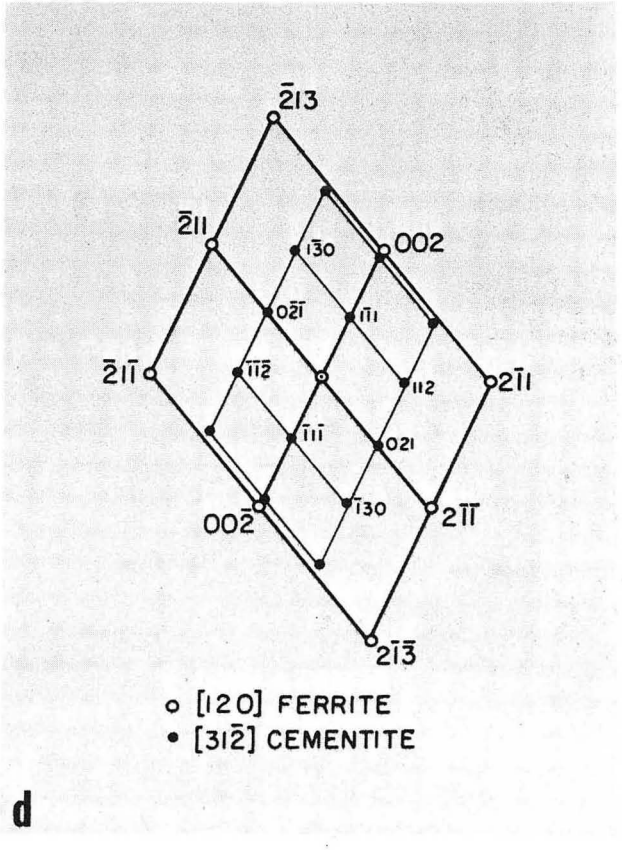

Fig. 7

XBB 765 3914

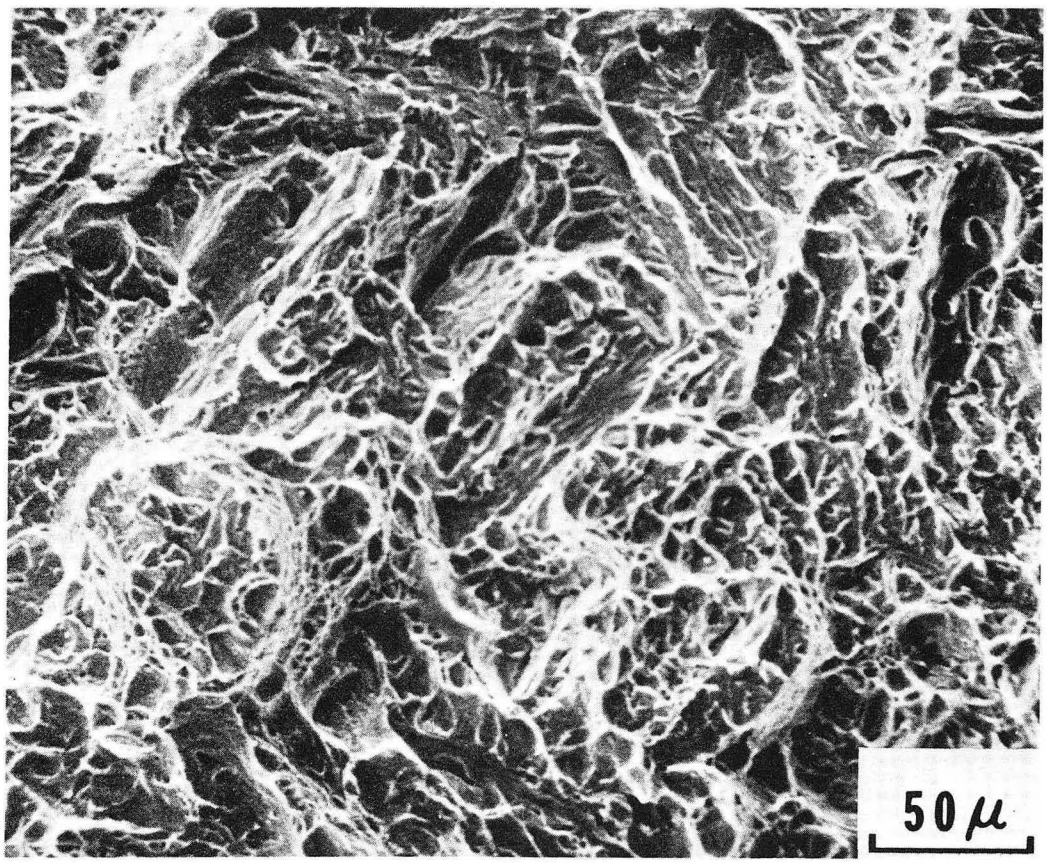

XBB 765-3931-A

Fig. 8

XBB 7410-7031-A

Fig. 9

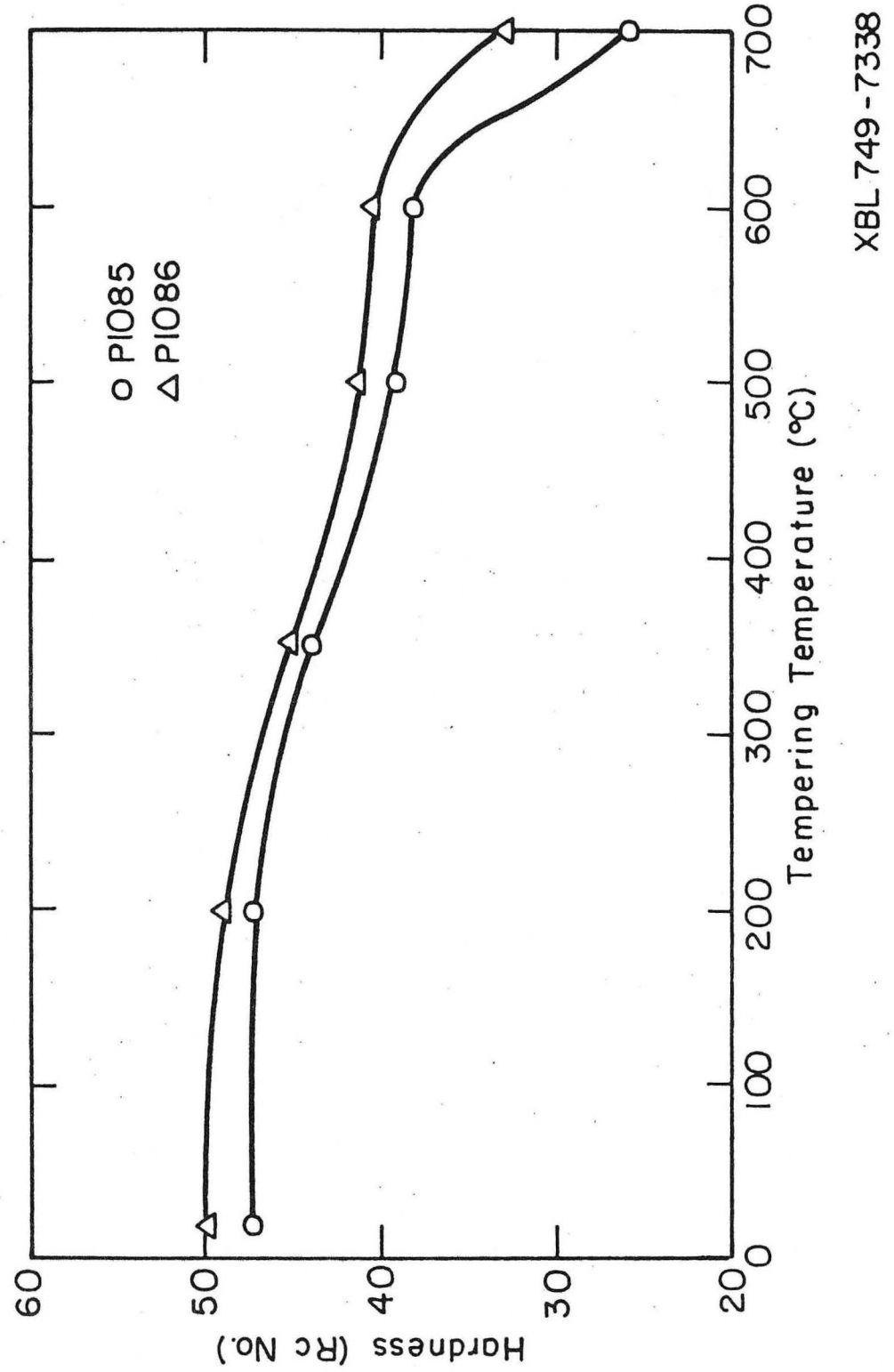
Hardness (Rc No.)
60
50
40
30
20
0
100
200
300
400
500
600
700
Tempering Temperature (°C)
O P1085
Δ P1086
XBL 749-7338

Fig. 10

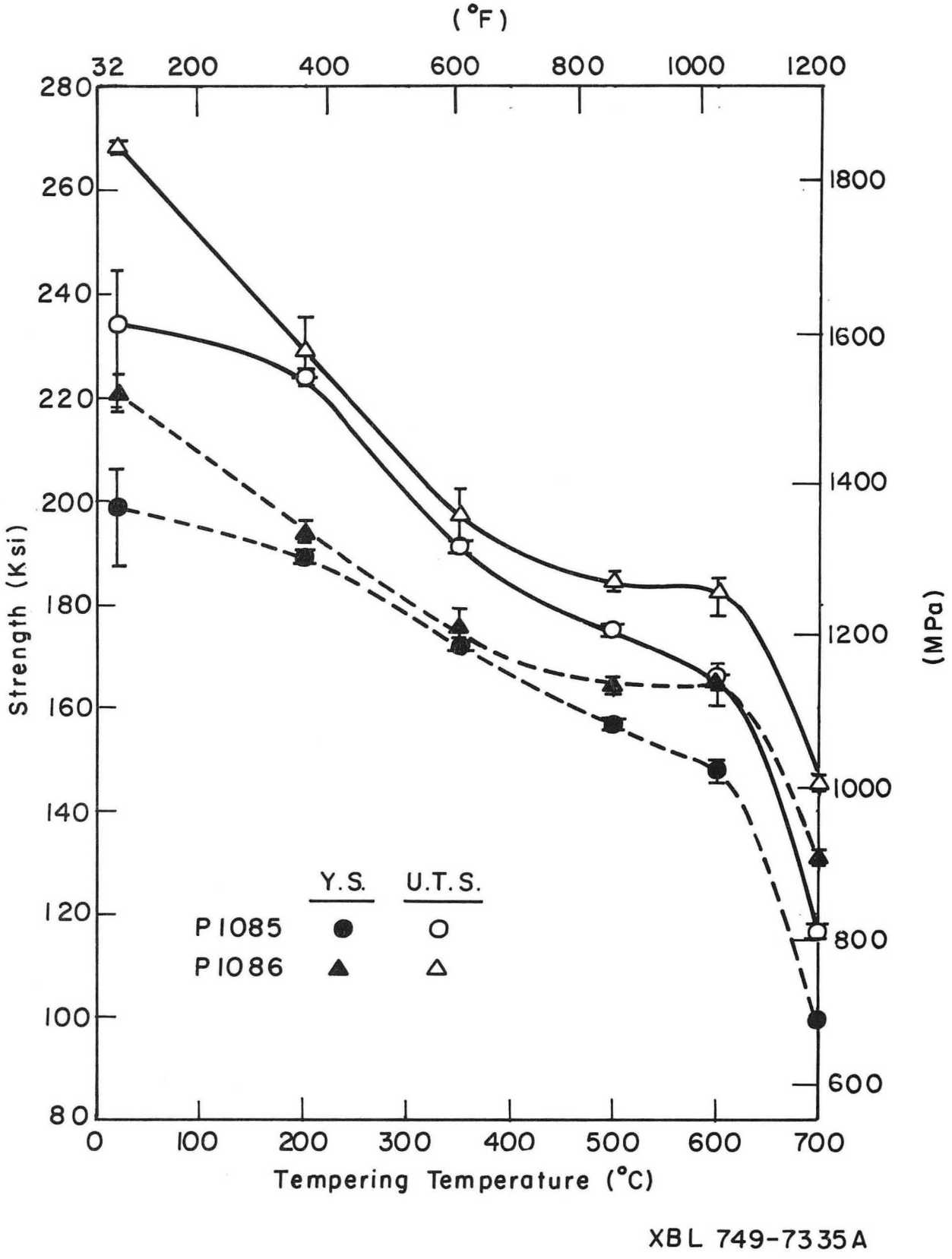
(°F)
32
200
400
600
800
1000
1200
280
260
240
220
200
180
160
140
120
100
80
1800
1600
1400
1200
1000
800
600
Strength (Ksi)
(MPa)
Y.S.
U.T.S.
P1085
P1086
0
100
200
300
400
500
600
700
Tempering Temperature (°C)
XBL 749-7335A

Fig. 11(a)

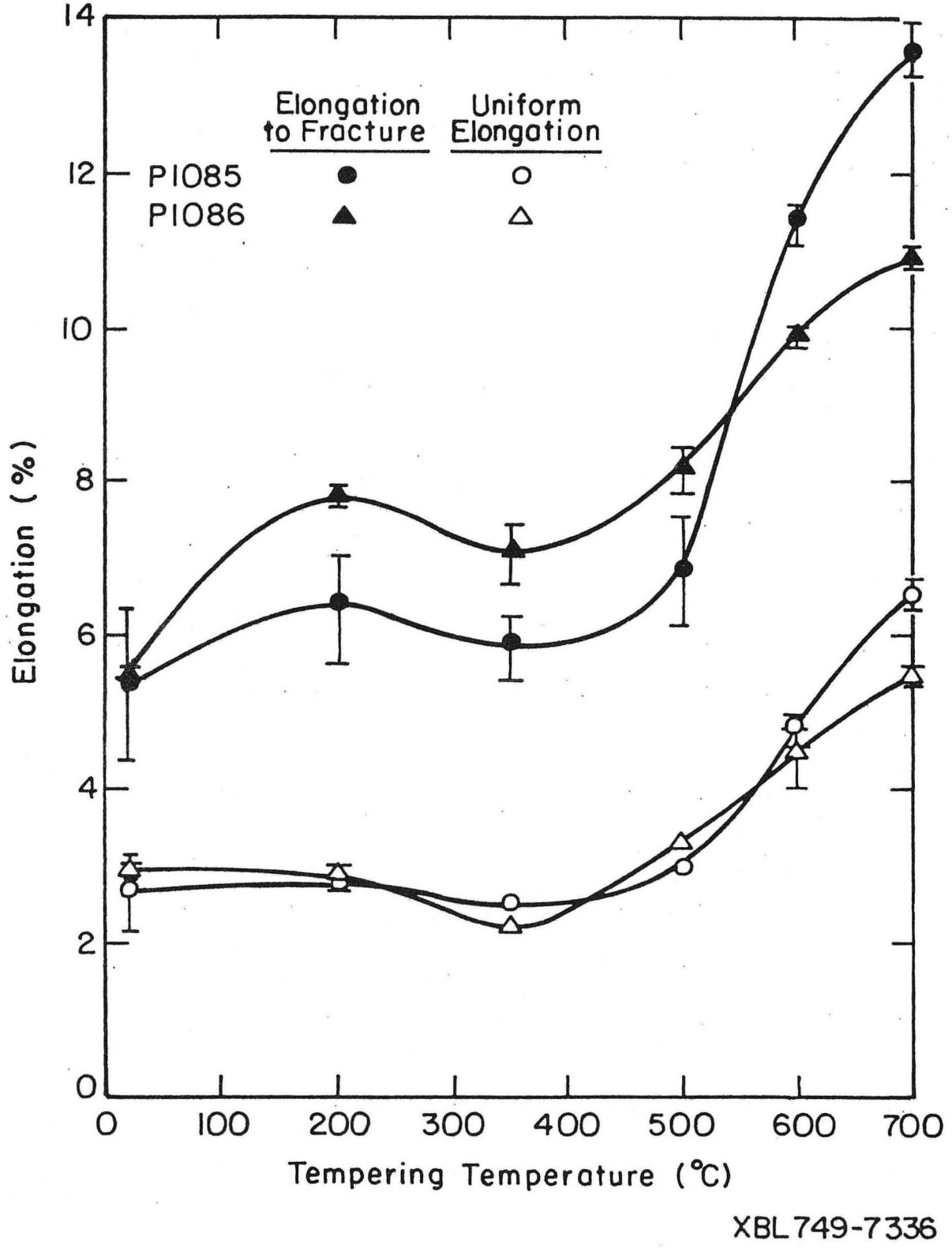
Elongation to Fracture
Uniform Elongation
P1085
P1086
Elongation (%)
Tempering Temperature (°C)
0
2
4
6
8
10
12
14
0
100
200
300
400
500
600
700
XBL749-7336

Fig. 11 (b)

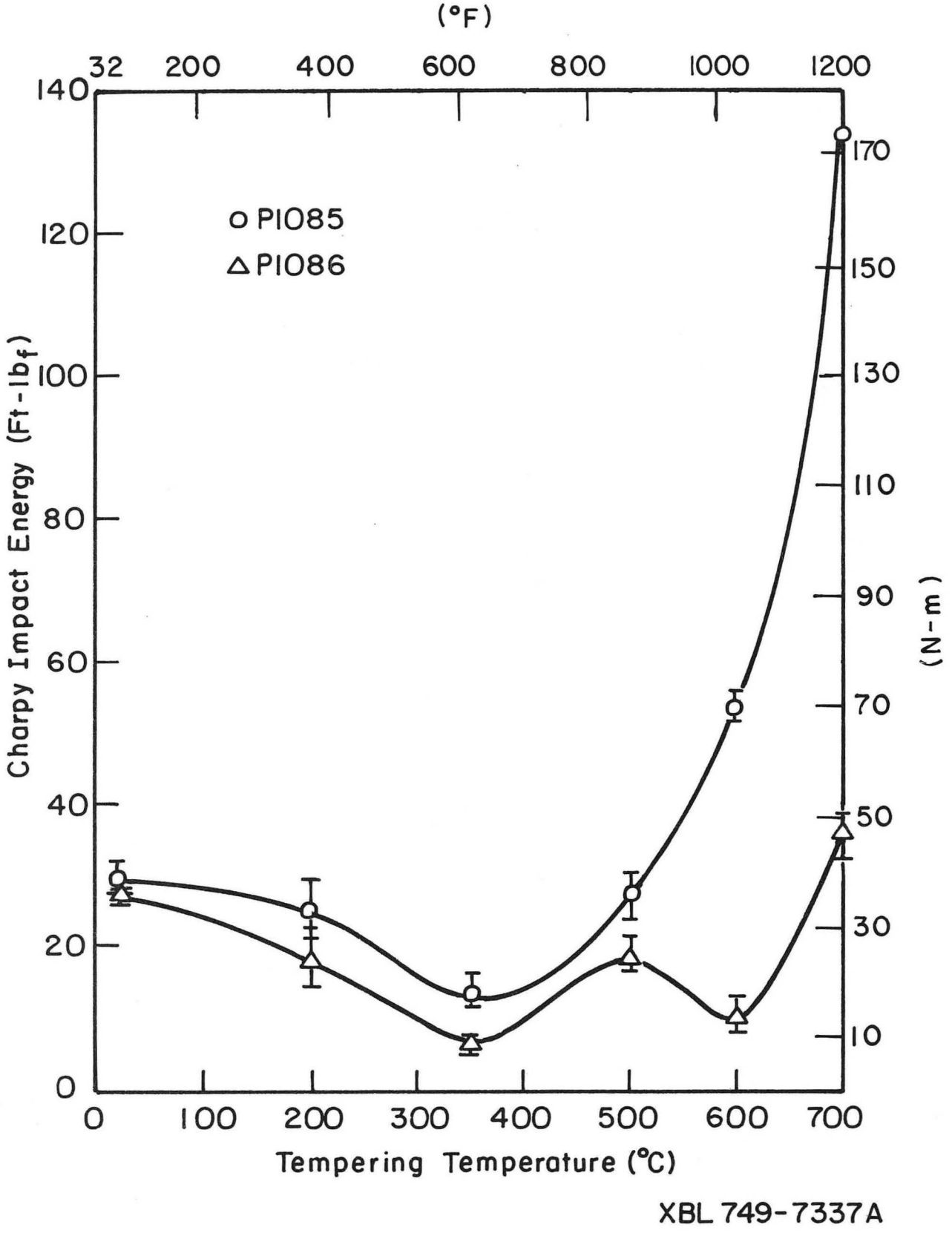
(°F)
32
200
400
600
800
1000
1200
140
120
100
80
60
40
20
0
170
150
130
110
90
70
50
30
10
o P1085
△ P1086
Charpy Impact Energy (Ft-lbf)
(N-m)
0
100
200
300
400
500
600
700
Tempering Temperature (°C)
XBL 749-7337A

Fig. 12

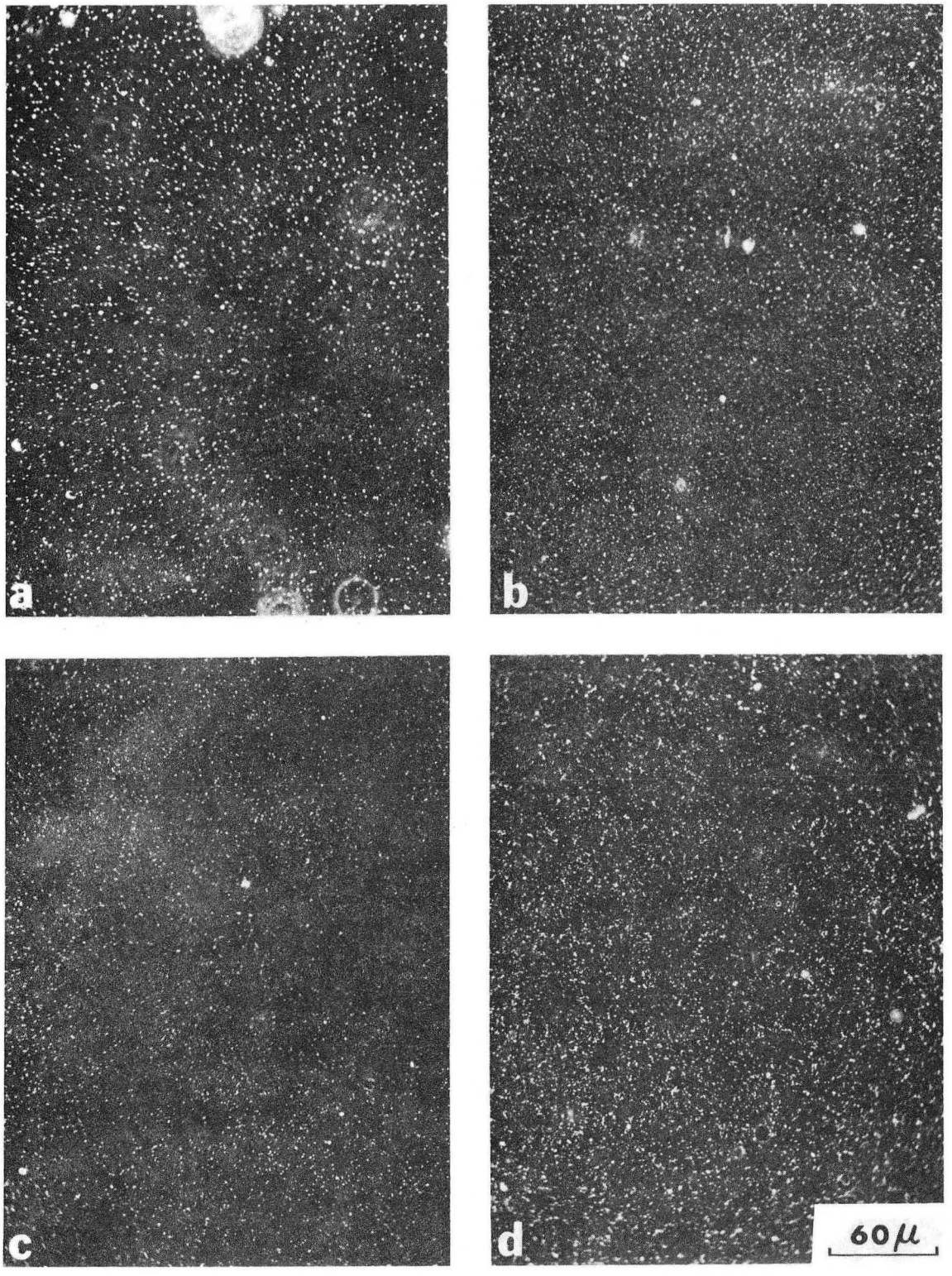

XBB 765-3262

Fig. 13

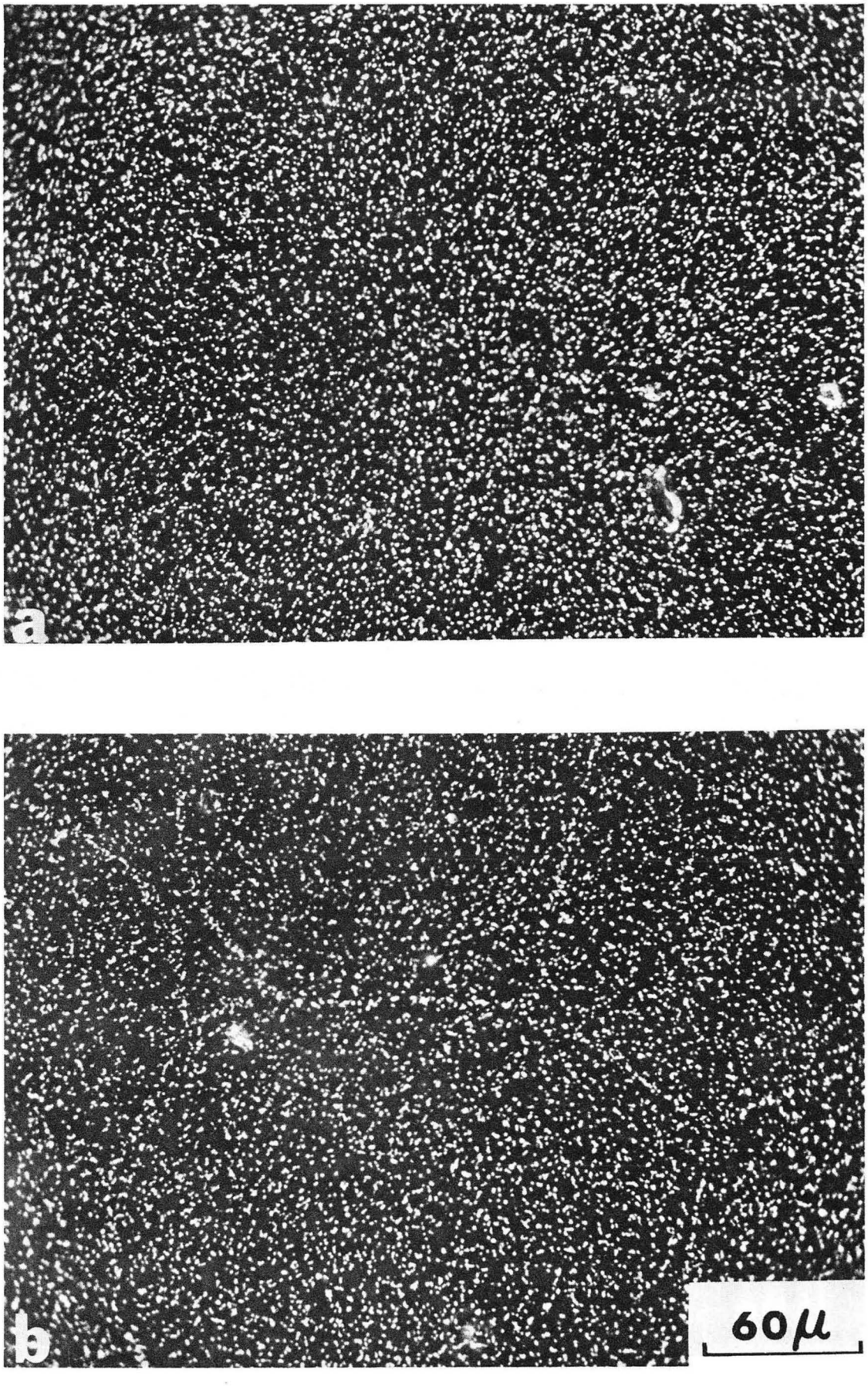

Fig. 14

XBB 765 3261

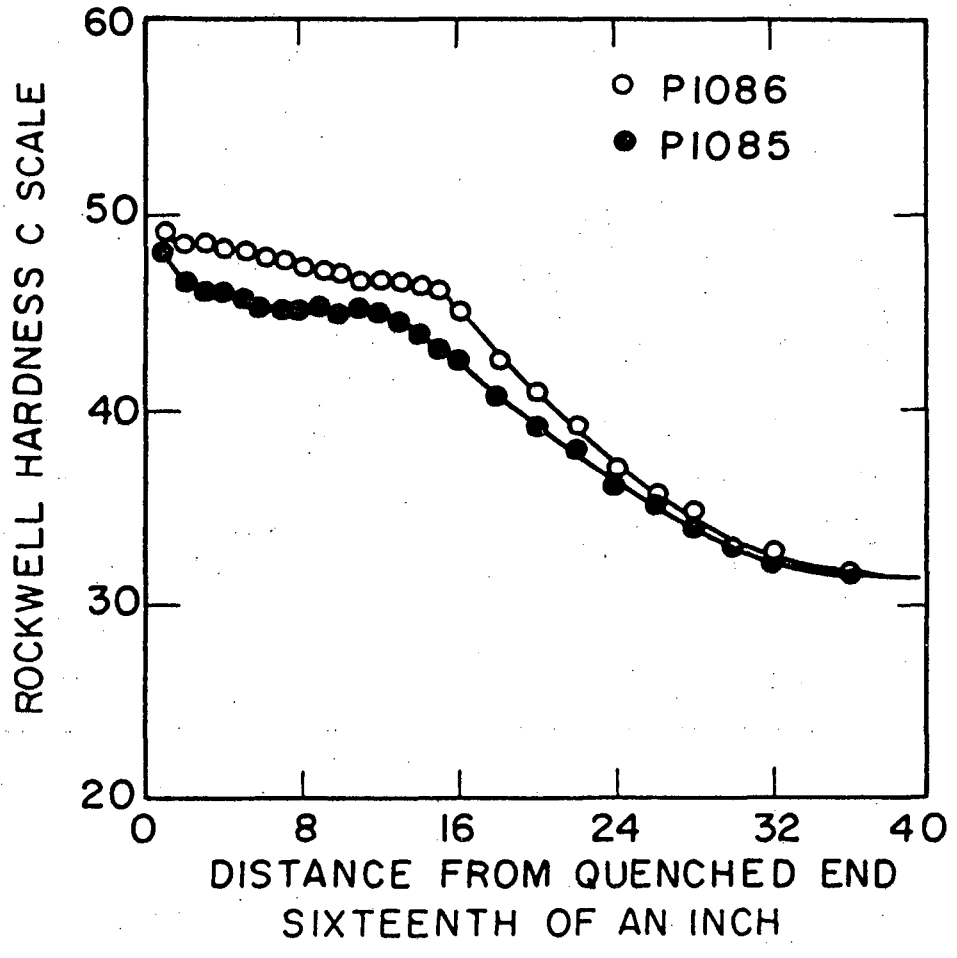
60
50
40
30
20
0
8
16
24
32
40
P1086
P1085
ROCKWELL HARDNESS C SCALE
DISTANCE FROM QUENCHED END
SIXTEENTH OF AN INCH
XBL764-6745

Fig. 15

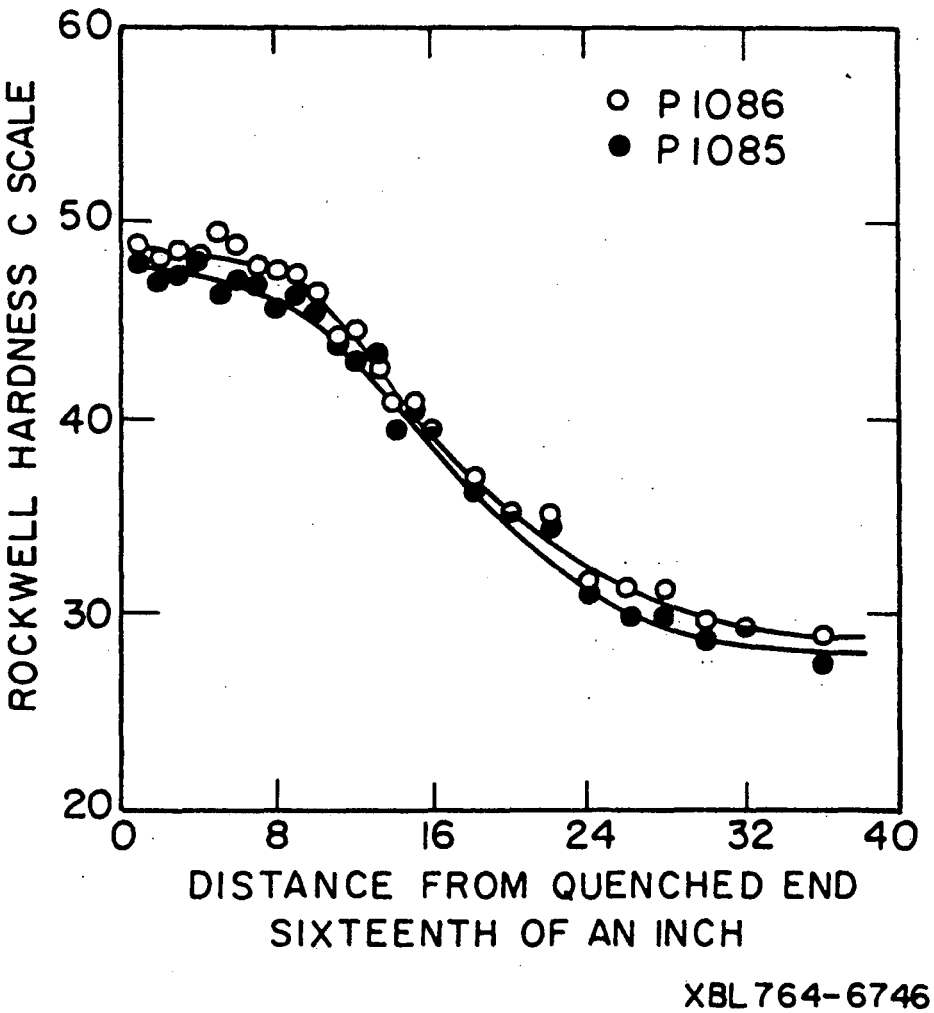
60
50
40
30
20
ROCKWELL HARDNESS C SCALE
P1086
P1085
0
8
16
24
32
40
DISTANCE FROM QUENCHED END
SIXTEENTH OF AN INCH
XBL764-6746

Fig. 16

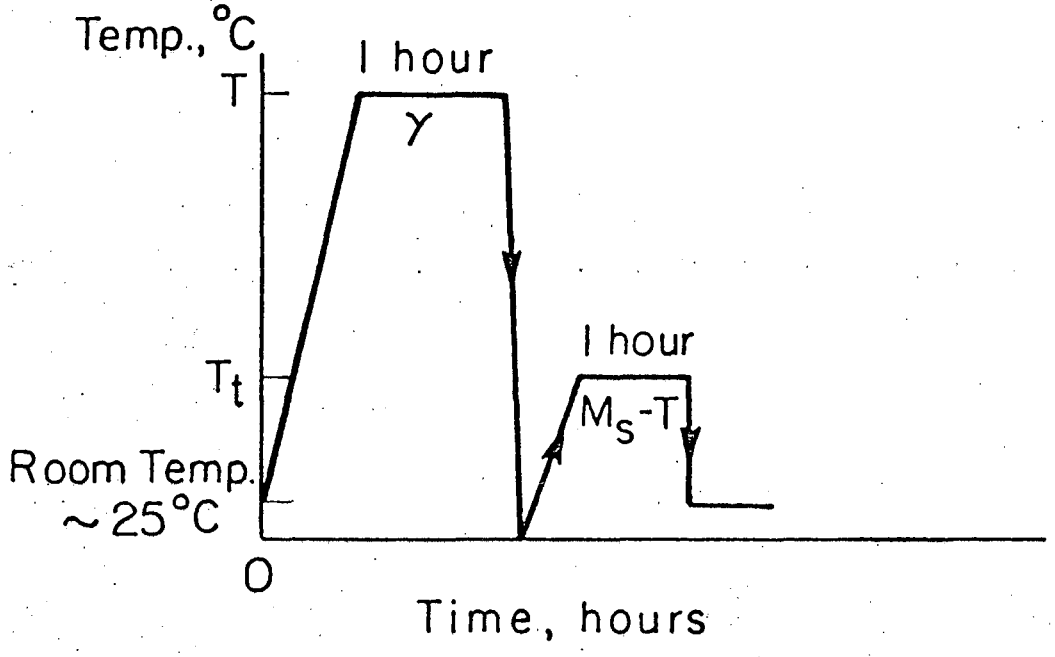

(a)

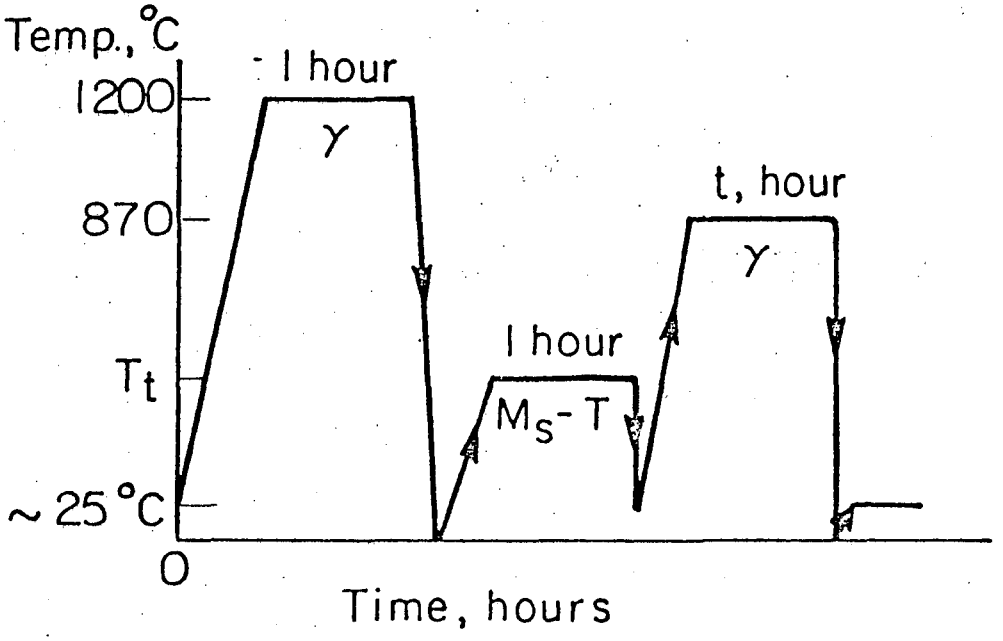

(b)

XBL 761-6276

Fig. 17

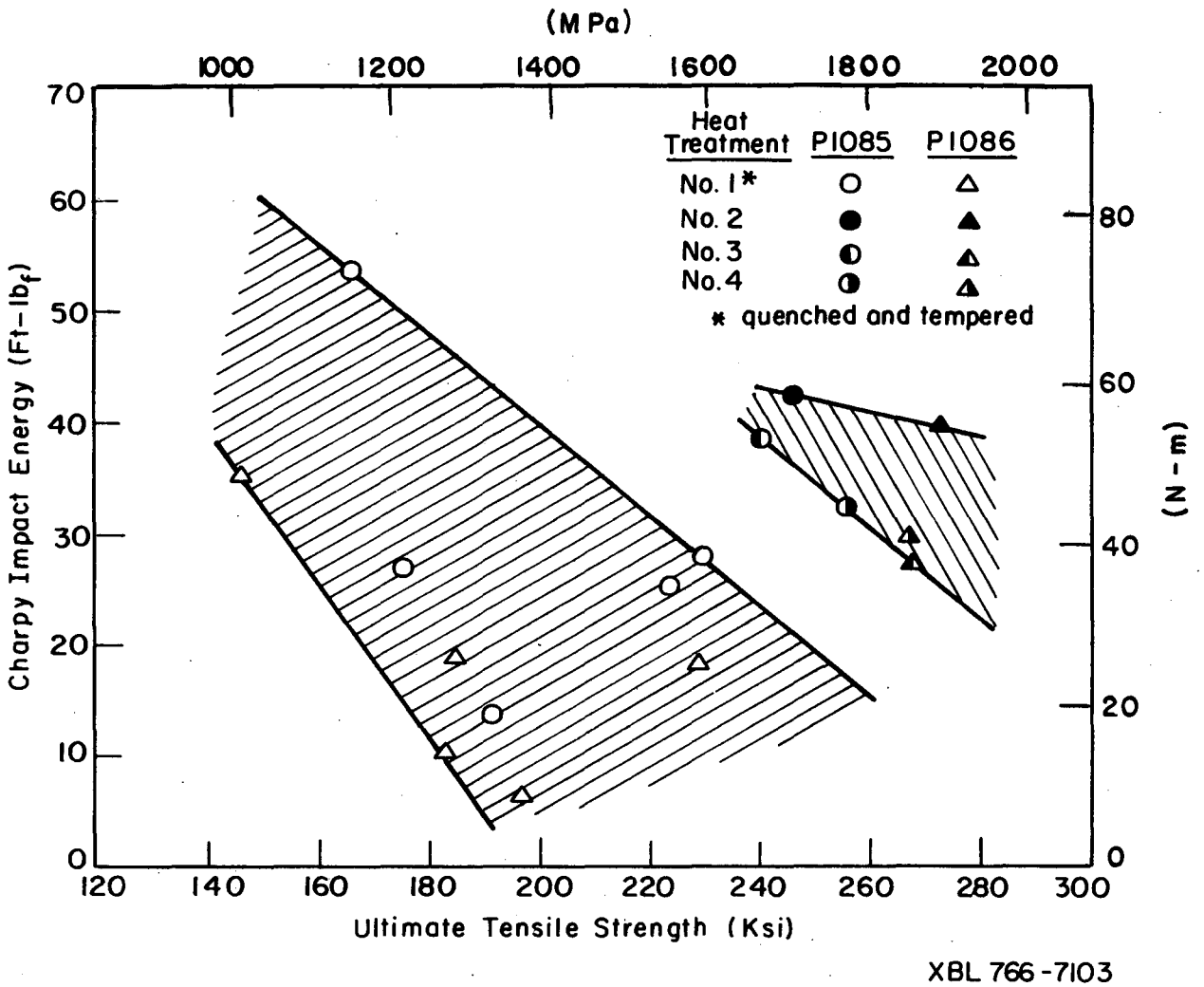
(M Pa)
1000
1200
1400
1600
1800
2000
Heat Treatment
P1085
P1086
No. 1*
No. 2
No. 3
No. 4
* quenched and tempered
Charpy Impact Energy (Ft-lb$_f$)
(N - m)
70
60
50
40
30
20
10
0
80
60
40
20
0
120
140
160
180
200
220
240
260
280
300
Ultimate Tensile Strength (Ksi)
XBL 766-7103

Fig. 18

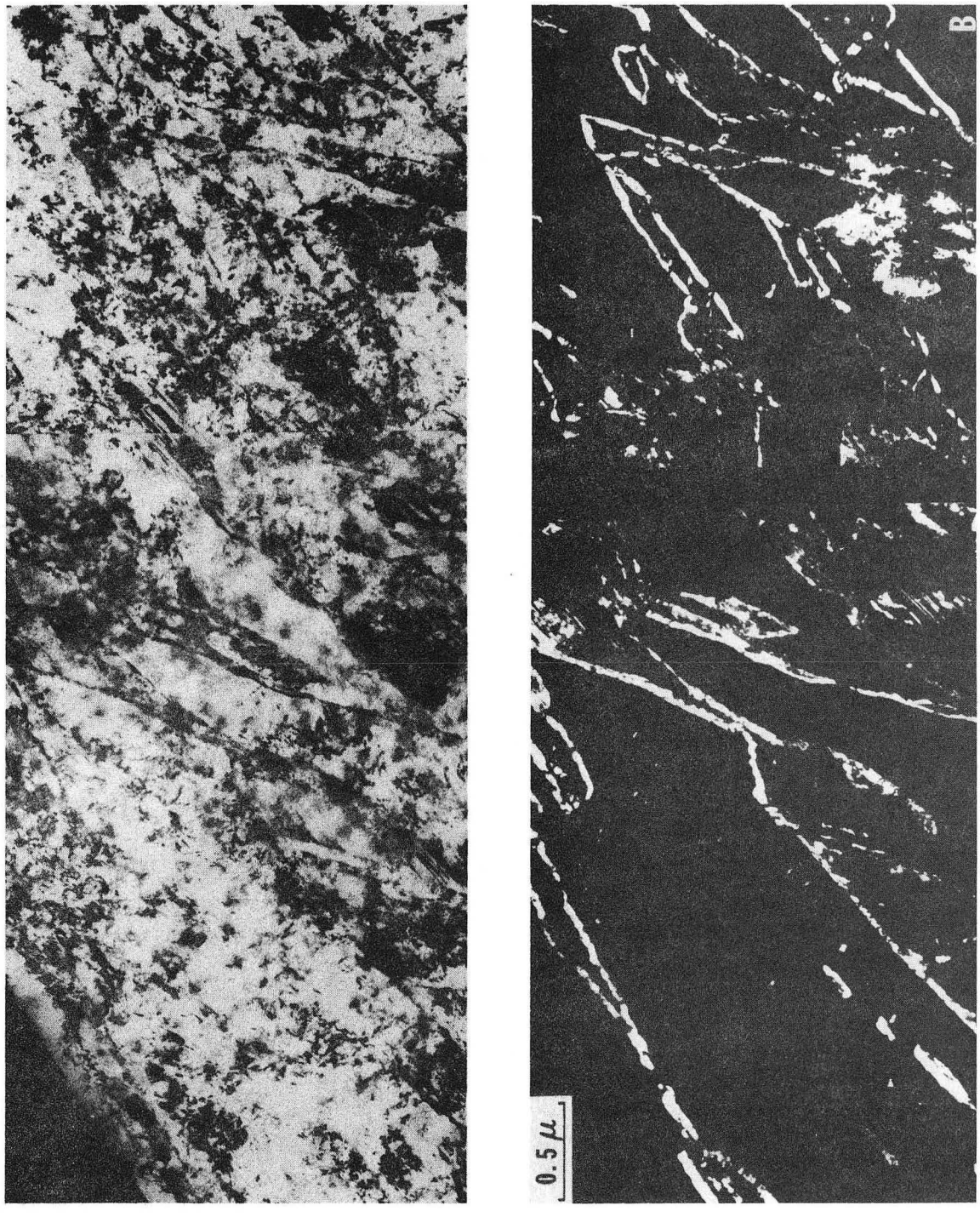

XBB 758-5825

Fig. 19

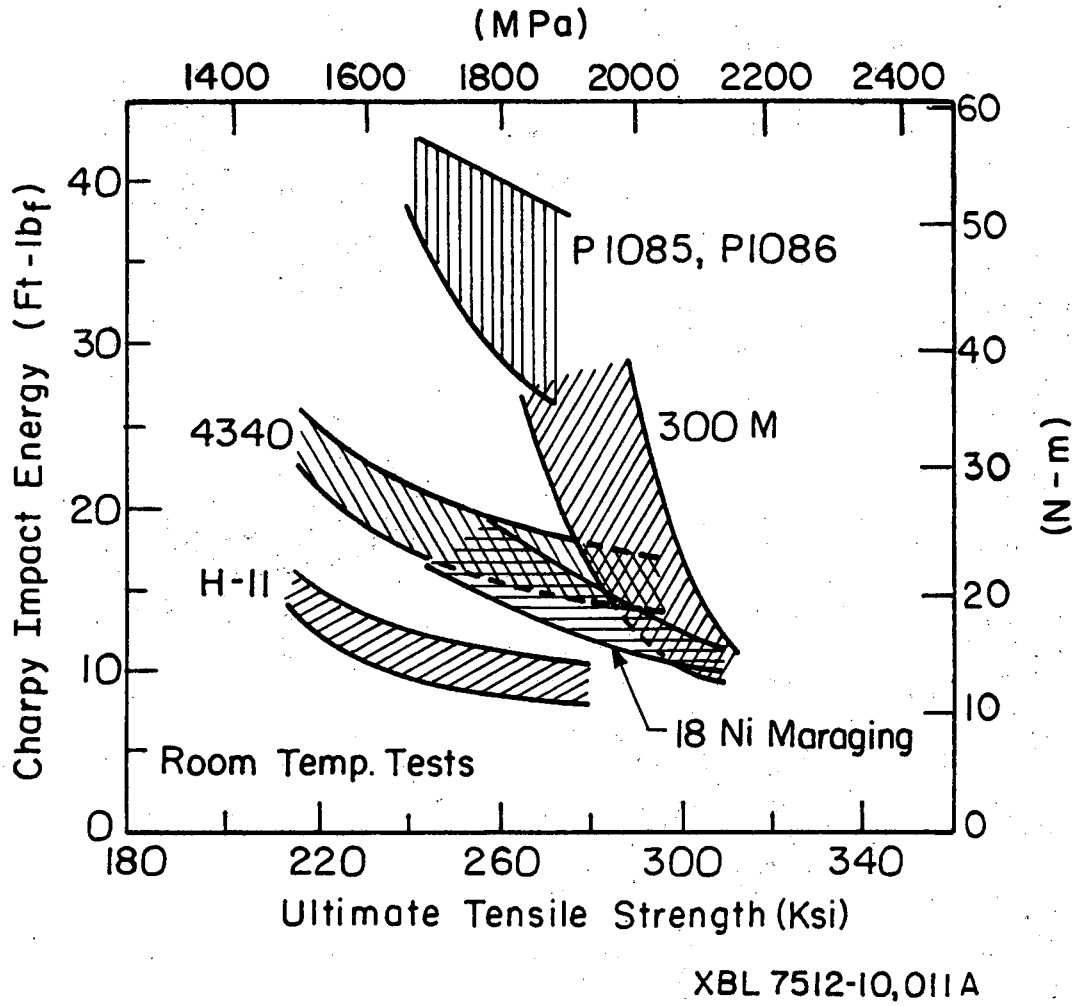
(MPa)
1400
1600
1800
2000
2200
2400
Charpy Impact Energy (Ft-lbf)
40
30
20
10
0
60
50
40
30
20
10
0
(N-m)
P1085, P1086
300 M
4340
H-11
18 Ni Maraging
Room Temp. Tests
180
220
260
300
340
Ultimate Tensile Strength (Ksi)
XBL 7512-10,011A

Fig. 20

TECHNICAL INFORMATION DEPARTMENT
LAWRENCE BERKELEY LABORATORY
UNIVERSITY OF CALIFORNIA
BERKELEY, CALIFORNIA 94720